THE ASTROPHYSICAL JOURNAL, 495:698–717, 1998 March 10

FAR-ULTRAVIOLET SPECTRA OF STARBURST GALAXIES: STELLAR POPULATION AND THE KINEMATICS OF THE INTERSTELLAR MEDIUM[1]

ROSA M. GONZÁLEZ DELGADO AND CLAUS LEITHERER
Space Telescope Science Institute, 3700 San Martin Drive, Baltimore, MD 21218; gonzalez@stsci.edu, leitherer@stsci.edu
TIMOTHY HECKMAN[2]
Department of Physics & Astronomy, Johns Hopkins University, Baltimore, MD 21218; heckman@pha.jhu.edu
JAMES D. LOWENTHAL
University of California, Lick Observatory, Santa Cruz. CA 95064; james@lick.ucsc.edu
HENRY C. FERGUSON
Space Telescope Science Institute, 3700 San Martin Drive, Baltimore, MD 21218; ferguson@stsci.edu
AND
CARMELLE ROBERT
Université Laval, Departement de Physique, Ste-Foy, PQ, G1K 7P4, Canada, and Observatoire du Mont Mégantic; carobert@phy.ulaval.ca
Received 1997 June 13; accepted 1997 October 20

ABSTRACT

The far-ultraviolet spectra of the four starburst galaxies NGC 6090, Mrk 66, Mrk 1267, and IRAS 0833+6517 were observed with the Hopkins Ultraviolet Telescope during the Astro-2 mission. Additional data were obtained for IRAS 0833+6517 with the Goddard High-Resolution Spectrograph (GHRS) on the *Hubble Space Telescope*. We analyze the observations in terms of the stellar content and the kinematics of the interstellar medium, and we discuss the implications of these results for the interpretation of the ultraviolet spectra of high-redshift galaxies.

Evolutionary synthesis models are used to constrain the star formation history from the absolute ultraviolet flux and from the stellar components of the absorption lines of Si IV and C IV, and from the far-ultraviolet lines O VI + Lyβ + C II. The spectral energy distributions from these models are used as inputs for the photoionization code CLOUDY to predict [O III]/Hβ and column densities of the cool component of the ionized gas (Si II and C II) associated with the H II region. The results indicate continuous star formation during about 9 Myr, or, alternatively, bursts with ages between 3 and 6 Myr, and a mass consistent with that estimated from the Hα flux. Evidence for significant dilution by a field star population is found in all galaxies except NGC 6090.

Most of the interstellar absorption lines are saturated. Their equivalent widths indicate a large velocity dispersion in the gas. Other evidence for large-scale motions of the interstellar gas comes from blueshifts of several hundred km s^{-1} with respect to the systemic velocity in the interstellar lines of NGC 6090, Mrk 66, and IRAS 0833+6517. These outflows are most likely driven by the starburst.

Lyα was detected in emission in three of the galaxies (NGC 6090, Mrk 66, and IRAS 0833+6517). The dereddened Lyα/Hβ ratio in IRAS 0833+6517 is close to the recombination value, indicating that extinction is more important than multiple resonant scattering effects. However, the GHRS spectrum of IRAS 0833+6517 clearly shows that the emission profile of Lyα is asymmetric, the blue wing being absorbed by neutral gas. This indicates that the velocity structure of the neutral gas and the scattering by H I atoms can also play an important role in the escape of the Lyα photons.

Subject headings: galaxies: evolution — galaxies: ISM — galaxies: starburst — galaxies: stellar content — ISM: kinematics and dynamics — ultraviolet: galaxies

1. INTRODUCTION

One of the most important present astrophysical issues is understanding the formation and evolution of galaxies. One way to address this problem is through the study of high-redshift objects. Any high-redshift object can be considered as a star-forming galaxy if it looks like a galaxy and is identified by spectral features consistent with those arising from young stars (types O, B, and A). Many observational programs to detect such objects have been carried out during the past few years (e.g., Pritchet & Hartwick 1990; Lowenthal et al. 1990; Djorgovski 1992; Steidel & Hamilton 1993; McCarthy 1993; Wolfe 1995; Thompson, Djorgovski, & Trauger 1995). A small number of star-forming galaxy candidates have been found at high redshift near QSOs or damped Lyα systems (e.g., Lowenthal et al. 1991; Moller & Warren 1993; Lowenthal et al. 1995; Francis et al. 1996; Djorgovski et al. 1996; Hu & McMahon 1996; Malkan, Teplitz, & McLean 1995) or serendipitously (e.g., Ebbels et al. 1996; Trager et al. 1997; Franx et al. 1997; Yee et al. 1996). However, it is only recently that the class of 10 m telescopes have allowed spectroscopic confirmation of large numbers of star-forming galaxies at high redshifts, as selected by their broadband colors (Steidel et al. 1996;

[1] Based on observations made with the Hopkins Ultraviolet Telescope and the NASA/ESA *Hubble Space Telescope*, obtained at the Space Telescope Science Institute, operated by AURA, Inc., under NASA contract NAS5-26555.

[2] Adjunct astronomer at the Space Telescope Science Institute.

Lowenthal et al. 1997). Many of these high-redshift galaxies show weak or absent Lyα emission, a strong UV continuum, compatible with large star formation rates, and absorption features that are quite similar to those found in local starburst galaxies. Low-ionization absorption lines, such as Si II λ1260, O I λ1302, Si II λ1304, C II λ1335, Si II λ1527, Fe II λ1608, and Al II λ1670, which are produced in the interstellar medium, are detected in the spectra; but so are higher ionization lines, such as Si IV λ1400 and C IV λ1550. All these characteristics make the high-redshift galaxies quite similar to nearby starbursts. However, the P Cygni profiles of the high-ionization metallic lines produced in the stellar wind of massive stars look weaker than in most nearby starbursts. This could be an effect of low metallicity at high redshift, since the strength of the stellar wind lines are metallicity dependent (Robert et al. 1997; Walborn et al. 1995). One exception is the galaxy MS 1512−cB58 (Yee et al. 1996). This is the brightest starburst known at high redshift (Ellingson et al. 1996). C IV and Si IV absorption lines look stronger here than in other high-redshift galaxies, and appear to be quite similar to those of local starbursts. Since the metallicity is expected to be lower than in nearby starbursts, a younger age, an upper-limit mass cutoff (M_{up}), or a flatter initial mass function (IMF) could be required to explain the C IV and Si IV in this high-redshift galaxy.

The ultraviolet (UV) continuum in high-redshift galaxies is quite red, and a large (1 to 3 mag) extinction correction is required to match the continuum slope with the predicted $\lambda^{-2.6}$ law derived from evolutionary synthesis models (Leitherer & Heckman 1995). These inferences are based on the uncertain assumption that in these high-redshift galaxies, the nature of the dust and the IMF is similar to that in nearby starbursts. However, the overall similarities of the UV spectra of nearby and distant star-forming galaxies are so compelling that local starburst galaxies make very good laboratories in which to explore spectroscopic techniques in the UV that can be used to study high-redshift galaxies, and ultimately star formation and the evolution of galaxies in the early universe.

Four nearby starburst galaxies were selected for observation with the Hopkins Ultraviolet Telescope (HUT) during the Astro-2 mission (Davidsen et al. 1992; Kruk et al. 1995). The main goal was a direct measurement of the escaping Lyman continuum flux. Because of the similarities between local starburst galaxies and high-redshift galaxies, and also because the large aperture of HUT can mimic the high-redshift situation rather well (even a narrow slit encompasses the entire central several starbursts), a direct measurement of the far-UV flux should be very useful in assessing the importance of star-forming galaxies for the ionization of the early universe (Miralda-Escudé & Ostriker 1990). In a previous paper, we derived 2 σ upper limits for the flux at 900 Å for each galaxy (Leitherer et al. 1995a). Comparison with stellar population synthesis models suggests that at most only a few percent of the ionizing photons can escape from these starburst galaxies. The implication is that young protogalaxies may not provide the Lyman continuum photons for the ionization of the early universe (see also Deharveng et al. 1997; Hurwitz et al. 1997).

Until now, no local starburst galaxy has been observed in the far-UV; thus, these observations give us the opportunity to explore new spectroscopic techniques in the far-UV that can later be applied to the study of the star formation history in high-redshift star-forming galaxies, where the far-UV emission is shifted to the near-UV or the optical. In fact, an absorption feature between 1010 Å and 1060 Å was detected in the spectra of these starburst galaxies. This can be attributed to the lines Lyβ, O VI λ1032, 1038, and C II λ1036, 1037. Evolutionary synthesis models of these lines have been performed (González Delgado, Leitherer, & Heckman 1997; hereafter Paper I). These were based on a stellar library built with spectra of O and B stars, which were used as inputs to an evolutionary synthesis code to predict the line profiles of O VI + Lyβ + C II. O VI is a very sensitive indicator for the presence or absence of O stars, which show a P Cygni profile. Lyβ and C II are very sensitive indicators for B stars. If a population younger than 1 Gyr is present in a galaxy, a strong stellar feature will be observed, from O VI if the dominant population are O stars or from Lyβ + C II if the feature is dominated by B stars.

In § 2 we describe the observations, and § 3 deals with the determination of the reddening through the UV continuum flux distribution. Section 4 presents a study of the stellar population using C IV, Si IV, and O VI profile synthesis techniques, and also the absolute flux at 1500 Å. Section 5 addresses the interstellar absorption lines and the kinematics of the interstellar medium. The Lyα emission and the effect of the extinction and gas absorption in the Lyα/Hβ ratio are discussed in § 6. The implications are taken up in § 7, and a summary and conclusions are given in § 8.

2. OBSERVATIONS

The initial motivation for far-UV observations of starburst galaxies was to study their Lyman continuum. The observations were performed with HUT during the Astro-2 mission in 1995 March, covering 820 Å to 1840 Å with a moderate resolution (R = 400 at 1200 Å). We selected four starburst galaxies that met the following criteria: (1) a large enough redshift to separate the starburst Lyman edge from the Galactic Lyman edge (thus the galaxies have $cz \geq 5000$ km s^{-1}); (2) large UV flux at 1500 Å; (3) strong Hα emission, indicating an intense source of ionizing radiation within each galaxy; and (4) low Galactic foreground extinction. The galaxies selected were NGC 6090, Mrk 66, Mrk 1267, and IRAS 0833+6517. Table 1 presents a summary of the properties of these galaxies. The Galactic foreground extinction was derived from the observed H I columns (Stark et al. 1992) and assuming $N_{\rm H\,I}/E(B-V) = 4.93 \times 10^{21}$ cm^{-2}. The values are given in Table 2.

The spectra were taken through circular apertures with diameters of 12″ and 20″, except for Mrk 66, which was observed through the large aperture only. 12″ corresponds to 3.8, 3.8, 4.4, and 5.8 Kpc for IRAS 0833+6517, Mrk 1267, Mrk 66, and NGC 6090, respectively. Because of centering uncertainties in the aperture and the resulting absolute flux uncertainties, we have taken the mean spectra of the two apertures. The mean value of the flux in the averaged spectra are 29% (NGC 6090), 9% (IRAS 0833+6517), and 3% (Mrk 1267) lower than the mean values in the spectra taken through the larger aperture. The small difference between the fluxes in the two apertures indicates that the UV sources do not extend beyond 12″. We have compared the continuum flux at 1350 Å and 1450 Å with the *IUE* flux given at these wavelengths by Kinney et al. (1993) and Margon et al. (1988). The *IUE* fluxes are about 30%, 50%, 3%, and 4% larger than the HUT fluxes for NGC 6090, Mrk 66, Mrk 1267, and IRAS 0833+6517,

TABLE 1

GALAXY PROPERTIES [a]

Name	Type	V (km s^{-1})	[O III]$_{5007}$/Hβ	Metallicity $Z_\odot$	Hα Flux (erg s^{-1} cm^{-2})	1″ (pc)
IRAS 0833+6517.....	SB Nuc	5608	1.8	0.60	1.3×10^{-12}	378
Mrk 1267.....	BCG	5780	1.25	0.48	2.0×10^{-13}	378
Mrk 66.....	BCG	6525	3.6	0.30	1.3×10^{-13}	441
NGC 6090.....	SB Nuc	8785	0.7, 1.5	0.76	6.8×10^{-13}	586

[a] Data from Calzetti & Kinney (1992), Hartmann et al. (1988), Margon et al. (1988), and Storchi-Bergmann, Kinney, & Challis (1995).

respectively. The difference in flux between the two apertures for NGC 6090 is due to the source being outside of the 12″ aperture for about a third of the integration time.

The zero point of the wavelength calibration was checked by fitting a Gaussian to the Galactic absorption lines. These lines were detected only in IRAS 0833+6517. From the fit to C II λ1335, we obtain a velocity shift of +45 km s^{-1} with respect to the nominal zero point. For the other three galaxies, we estimated the shift by fitting the geocoronal Lyβ. However, because this line fills the aperture in a way very different from the galaxies, this estimate does not necessarily give exactly the zero point of the wavelength calibration. The center values of the Lyβ geocoronal emission are 1025.3 Å, 1026.0 Å, 1025.8 Å, and 1025.2 Å for Mrk 1267, Mrk 66, NGC 6090, and IRAS 0833+6517, respectively. These imply a correction to the zero point of −123 km s^{-1}, +82 km s^{-1}, −23 km s^{-1}, and −152 km s^{-1}, respectively. More details about the observations and reduction of the data are given in Leitherer et al. (1995a).

Additional data for IRAS 0833+6517 were obtained with the *HST*. The galaxy was observed with the Goddard High-Resolution Spectrograph (GHRS) and the grating G140L, which has a nominal dispersion of 0.57 Å per diode, through the Large Science Aperture (LSA, 1.7 × 1.7 arcsec^2). One of the exposures, with an integration time of 4216 s, covers 1213 Å to 1499 Å, and three exposures were taken covering 1465 Å to 1752 Å, with a total integration time of 13,872 s. After standard pipeline processing, all the spectra were combined into a single spectrum covering 1213 Å to 1752 Å.

The instrumental spectral resolution for a point source observed through the LSA is 0.80 Å, but for an extended source this depends on the size of the UV source. Using the Galactic C II λ1335 interstellar absorption line, we determine that the instrumental resolution is better than 2.3 Å FWHM for IRAS 0833+6517. The center of the Gaussian fit to this line is 1334.4 ± 0.1 Å, giving an uncertainty in the zero-point wavelength calibration of 0.1 Å (23 km s^{-1}). The continuum flux in the GHRS spectrum is a factor of 3 lower than in the HUT spectrum. This difference reflects the aperture loss in the GHRS spectrum, and tells us that the UV source is more extended than 2″. WFPC2 images of the galaxy at 2200 Å show that most of the UV light is emitted by bright spots aligned in an internal bar extending 3 × 0.9 arcsec^2 (1.1 × 0.3 kpc^2). Diffuse emission is extended about 3″.6 (Robert et al. 1997).

The spectra were corrected for redshift with the values given in Table 1. Figure 1 shows the HUT spectra after a wavelet filtering was applied (Murtagh, Starch, & Bijaoui 1994), except for the galaxies IRAS 0833+6517 and NGC 6090, for which the spectrum shown is the original, rebinned every 4 pixels. The 1 σ error spectrum of the original data, assuming Poisson noise, is shown at the bottom. The S/N ratio at 1500 Å is 9, 4, 3, and 5 for IRAS 0833+6517, Mrk 1267, Mrk 66, and NGC 6090, respectively. The spectra are in the rest-frame wavelength for each galaxy. Figure 1 also shows the GHRS spectrum of IRAS 0833+6517 corrected for redshift and rebinned to 0.57 Å pixel^{-1}. The original spectra were oversampled by 0.25 pixel steps.

The most prominent absorption features seen in the spectra are Lyβ + O VI λ1032, 1038 + C II λ1036, Si II λ1260, O I + Si II λ1303, C II λ1335, Si IV λ1400, Si II λ1526, and C IV λ1550. The strongest emission features are the geocoronal Lyα and Lyβ, and also the intrinsic Lyα in emission. An exception is Mrk 1267, which has Lyα in absorption.

3. CONTINUUM FLUX DISTRIBUTION

Leitherer & Heckman (1995) have shown that the UV energy distribution for young starbursts is always very similar for a range in metallicity between 0.1 and 2 solar, IMF slope between 2.35 and 3.3, and upper cutoff mass between 30 and 100 $M_\odot$. This energy distribution can be fitted by a power law, $F_\lambda \propto \lambda^\beta$. The index β measures the slope of the continuum between 1200 and 1900 Å. It is almost constant, with values in the range −2.6 to −2.2 if the starburst is younger than 10 Myr. Thus, any deviation from the range of values predicted by the models can be attributed to reddening. Using the extragalactic extinction law derived by Kinney et al. (1994), Leitherer et al. (1996) find a relationship between the color excess and the change of the UV continuum slope produced by reddening,

TABLE 2

CONTINUUM SLOPE AND REDDENING

Name	Slope	$E(B-V)_{UV}$ (Kinney et al.)	$E(B-V)_{UV}$ (LMC)	$E(B-V)_{UV}$ (MW)	$E(B-V)_{Balmer}$	$E(B-V)_{Gal}$
IRAS 0833+6517 (HUT)	−0.85	0.19	0.17	0.40	0.52	0.08
IRAS 0833+6517 (GHRS).....	−1.70	0.10	...	...	0.52	0.08
Mrk 1267	−0.43	0.24	0.20	0.42	0.55	0.08
Mrk 66.....	−1.58	0.11	0.11	0.23	0.0	0.03
NGC 6090	−0.50	0.23	0.23	0.50	0.60	0.03

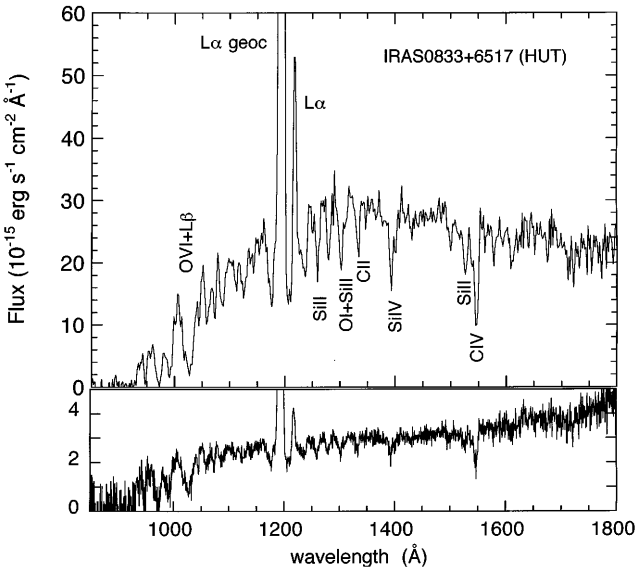

FIG. 1*a*

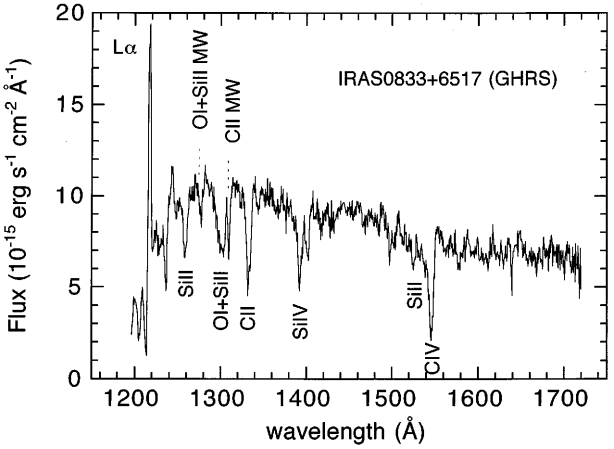

FIG. 1*b*

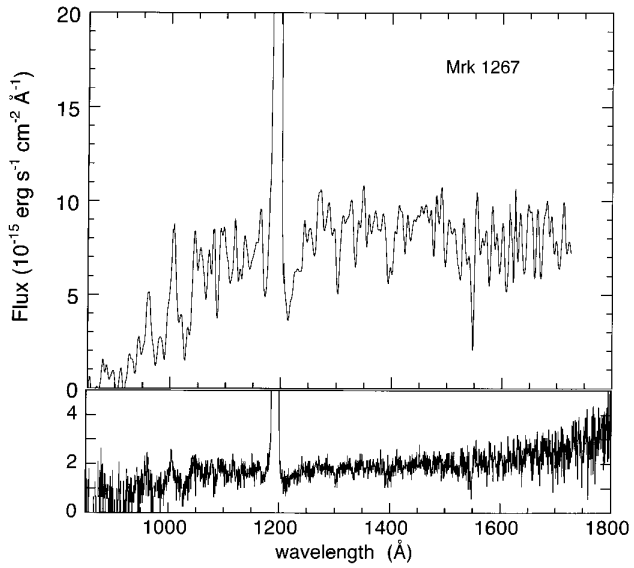

FIG. 1*c*

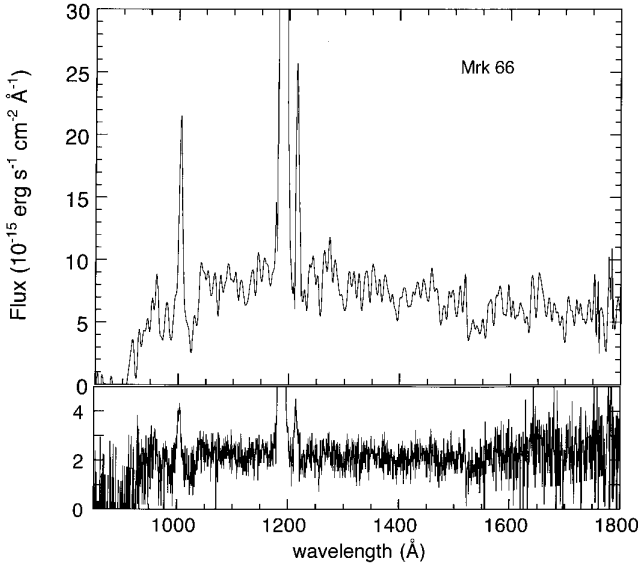

FIG. 1*d*

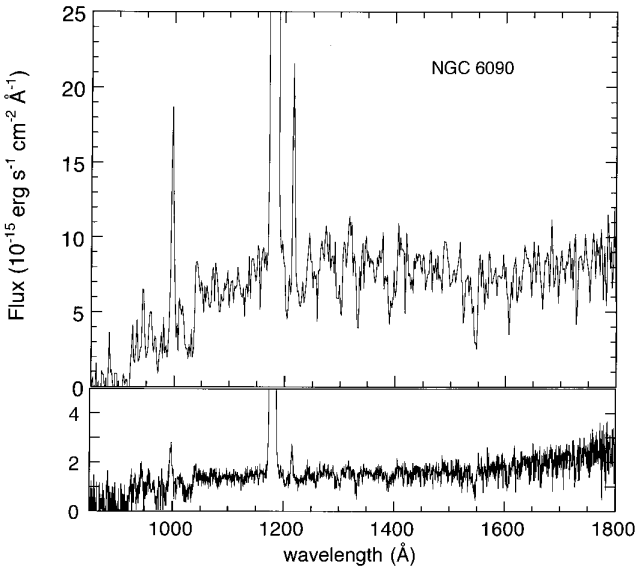

FIG. 1*e*

FIG. 1.—Ultraviolet spectra of the starburst galaxies at the rest wavelength. (*a*) IRAS 0833+6517 (HUT spectrum). (*b*) IRAS 0833+6517 (GHRS spectrum). (*c*) Mrk 1267. (*d*) Mrk 66. (*e*) NGC 6090. Lower panels in (*a*), (*c*), (*d*), and (*e*) show the 1 σ error spectrum calculated assuming Poisson noise.

$E(B-V) = 0.11\,\Delta\beta$, where $\Delta\beta$ is the difference between the observed and the predicted slope. This method of determining the reddening is based on the assumption that the starburst is dominated by only a young burst (less than 10 Myr old). If older bursts contribute significantly to the UV continuum, the slope would be flatter than -2.2, and the extinction determined in this way should be an upper limit to the real value.

We have derived the continuum slope by fitting a first-order polynomial in the ($\log F_\lambda$, $\log \lambda$) plane using different windows for the continuum. Table 2 gives the average value of the slope for each galaxy and the color excess derived. However, the color excess derived depends on the extinction law used. We have also checked that the reddening derived in this way gives similar results, within the errors, if we use the LMC extinction law instead of the law given by Kinney et al. (1994). However, the $E(B-V)$ values derived using the Milky Way (MW) extinction law instead of the Kinney or LMC law are larger by a factor of 2 (see Table 2).

Because Galactic extinction toward these galaxies is smaller than the reddening derived (see Table 2), the color excess indicates that some internal extinction affects the starburst. However, the reddening values derived using the UV continuum and the Kinney et al. (1994) or LMC extinction laws are lower than those derived using the Balmer decrement. This discrepancy between the extinctions derived from the two methods has previously been found by Fanelli, O'Connell, & Thuan (1988) and Calzetti, Kinney, & Storchi-Bergmann (1994). No significant difference is found between the two methods if the MW extinction law is assumed instead of the LMC or that of Kinney et al. (1994).

In the same way, we have derived the slope and the color excess of IRAS 0833+6517 using the GHRS spectrum. The slope is somewhat steeper ($\beta = -1.7$) and the color excess lower [$E(B-V) = 0.1$] than the value derived from the HUT spectrum, probably indicating a nonhomogeneous distribution of the dust and/or a change in the mean evolutionary state of the stellar population with the aperture size.

4. STELLAR POPULATION: LINE PROFILE SYNTHESIS AND ABSOLUTE FLUX SYNTHESIS

The most important stellar features seen in the near-UV region in the spectra of starburst galaxies are the resonance lines C IV λ1550 and Si IV λ1400. All O stars show a P Cygni profile in the C IV lines. In addition, all O supergiants show a P Cygni profile in Si IV (Walborn, Bohlin, & Panek 1985). In the far-UV, the most prominent stellar wind feature is the line O VI λ1032, 1038. All O and B0 stars develop a P Cygni profile or a blueshifted absorption feature in O VI (Morton 1979; Walborn et al. 1995). As with C IV and Si IV, the *profile* of O VI is a better indicator than its equivalent width of the properties of massive stars in a stellar cluster; this is because of the possible strong interstellar contribution in C IV and Si IV, and a possible blend of O VI with Lyβ and C II λ1036, 1037. Other ultraviolet lines that provide information on the stellar content in a starburst are the resonance line N V λ1240 and the recombination line He II λ1640. N V develops a strong P Cygni profile in the winds of all O and B0 stars. He II shows a broad emission profile, and it is formed in the very dense stellar winds of Wolf-Rayet (W-R) stars and O5–O3 supergiants (Leitherer, Robert, & Heckman 1995b; Robert et al. 1997).

Evolutionary synthesis models of a stellar population have been computed for C IV, Si IV, N V, and He II by Robert, Leitherer, & Heckman (1993) and Leitherer et al. (1995b), and for O VI + Lyβ + C II by González Delgado et al. (1997). These models are based on stellar libraries built with observations of O and B stars collected with *IUE* (for C IV and Si IV), *Copernicus*, and the HUT (for O VI + Lyβ + C II). These stellar libraries are used as inputs for an evolutionary synthesis code, and line profiles of C IV, Si IV, and O VI + Lyβ + C II are synthesized for different star formation histories (instantaneous burst and continuous star formation) and different assumptions about the IMF. These models have been computed for solar metallicity and with the assumption that the stars evolve from the zero-age main sequence (ZAMS) following the evolutionary tracks of Maeder (1990) for stars with masses larger than 15 $M_\odot$, and Maeder & Meynet (1988) for stars of between 1 and 15 $M_\odot$. More details of the models can be found in Leitherer & Heckman (1995), Leitherer et al. (1995b), and Paper I. Models at subsolar metallicity predict weaker C IV and Si IV P Cygni profiles than those generated using libraries of stars in the solar neighborhood (Robert et al. 1997). These models must be applied cautiously for metallicities lower than 1/3 solar.

In the following subsections, we use evolutionary synthesis models to study the evolutionary stage of the stellar population of the four starburst galaxies observed. First, we will apply the C IV, Si IV, and O VI + Lyβ + C II line profile synthesis technique. For C IV and Si IV, this technique has been successfully applied to starbursts (Leitherer et al. 1996; Conti, Leitherer, & Vacca 1996) and Seyfert 2 galaxies (Heckman et al. 1997; González Delgado et al. 1998). Our strategy is to find the best synthetic model that fits C IV and Si IV, and then to compare the synthetic O VI profile with the observations in order to infer the possible contribution of interstellar Lyβ and C II. In most cases, the line profile synthesis technique does not provide a unique solution. To distinguish which is the best solution and to further constrain the range of possible models, we use the UV continuum luminosity at 1500 Å. With this luminosity, we can predict the number of ionizing photons, Q, for each model. The predicted values are compared with the value derived from the Balmer recombination lines. We also use the equivalent width of the Balmer emission lines and the excitation ratio [O III]/Hβ. This ratio will be obtained by computing photoionization models, taking as ionizing spectrum the spectral energy distribution of the models. The reason for combining the UV continuum with the Balmer recombination lines and the excitation ratio is to ascertain whether the UV light is mainly the product of O or B stars. If hot stars produce the UV emission, models that fit the UV will correctly predict Q and the excitation ratio.

4.1. *IRAS 0833+6517*

4.1.1. C IV *and* Si IV *Line Profile Synthesis*

To find the best models that fit C IV and Si IV, we first use the GHRS data and then perform a consistency test with the HUT data.

A comparison of the profiles with those of NGC 1741, another starburst galaxy, indicates that the stellar absorption lines are not as strong in IRAS 0833+6517 as they are in NGC 1741. This indicates either that IRAS 0833+6517 is probably in a more advanced evolutionary stage than NGC 1741, which has an estimated age of 4–5 Myr (Conti et al. 1996), or that the IMF is steeper in IRAS 0833+6517 than

in NGC 1741, or that there is a dilution of the stellar lines in IRAS 0833+6517 due to an underlying population. Note that NGC 1741 was also observed with the GHRS at the same aperture as IRAS 0833+6517, and that it is at a similar distance as IRAS 0833+6517.

Because of a contribution from the *interstellar* C IV and Si IV (which are stronger in the starburst spectra than in the synthetic models), we do not fit the entire line profile. Instead, we select two wavelength windows, corresponding to the blue side of the wind profile, 1535–1542 Å (for C IV) and 1382–1390 Å (for Si IV), and to the red side, 1550–1560 Å (for C IV) and 1404–1409 Å (for Si IV), where the profiles are dominated by the stellar contribution. We compute the χ^2 parameter between the observations and every model, and the results are plotted for burst models as a function of age, upper mass limit cutoff, and slope of the IMF for C IV in Figures 2*a* and 2*b* and Si IV in Figures 2*c* and 2*d*, respectively. The same are plotted for continuous star formation (CSF) in Figures 3*a* and 3*b* for C IV and Figures 3*c* and 3*d* for Si IV, respectively. Each model is shown by a "bubble" in Figures 2 and 3, the size of the bubble being proportional to χ^2. A larger bubble size indicates a larger deviation between observations and models.

In the case of an instantaneous burst, we can exclude models younger than 5 Myr based on the values of χ^2 if the upper mass limit cutoff is higher than 40 $M_\odot$ or the IMF slope flatter than $\alpha = 3$ (IMF $\propto M^{-\alpha}$). Models with an age of 6 Myr are consistent with the data, but we cannot constrain the upper mass limit cutoff or the slope of the IMF, since for this age the most massive stars have already reached the supernova phase. Any age is compatible with the profiles if $M_{up} = 30\ M_\odot$ or $\alpha = 3.75$. For CSF models, we can exclude models of any age with an upper mass limit cutoff higher than 40 $M_\odot$ and a slope of the IMF flatter than $\alpha = 3$. Figures 4*a* and 4*b* show the profiles of C IV and Si IV for burst models, and Figs. 4*c* and 4*d* show these profiles for CSF models, for an age of 6 Myr.

Figure 5 compares the HUT spectrum with the GHRS spectrum rebinned at the same resolution as the HUT spectrum. An inspection of the C IV and Si IV profiles indicates no difference between the two spectra. Thus, the same conclusions that were found with the GHRS spectrum hold for the HUT spectrum. The differences between these spectra are the slope of the continuum (as we have noted previously, the HUT spectrum is flatter than the GHRS spectrum) and the strength of some interstellar lines (e.g., Si II λ1527 is stronger in the HUT spectrum than in the GHRS spectrum).

The most straightforward conclusion is that O stars must be present in the cluster of IRAS 0833+6517, in order to explain the blue wing of the C IV and Si IV lines, but these stars cannot be more massive than about 40 $M_\odot$, because M_{up} is less than 40 $M_\odot$ or the age is older than 5 Myr.

4.1.2. O VI + Lyβ + C II *Synthesis Profile*

Figure 6 shows the profile of the absorption feature between 1000 Å and 1060 Å. The equivalent width of this feature is 14.4 Å, and the minimum is at 1027 Å. The main

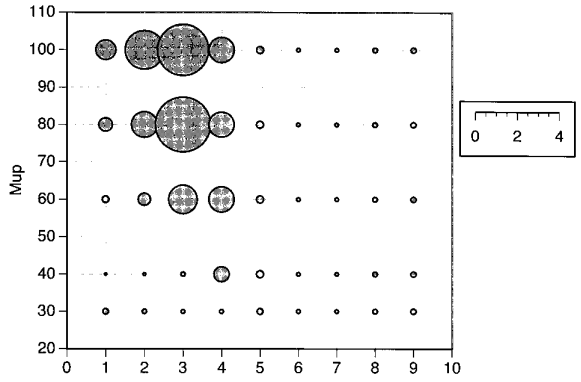

FIG. 2*a*

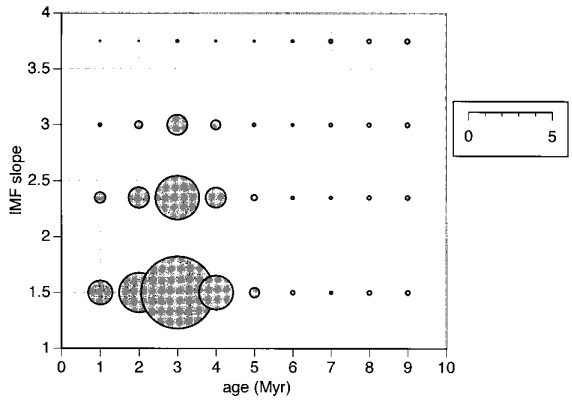

FIG. 2*b*

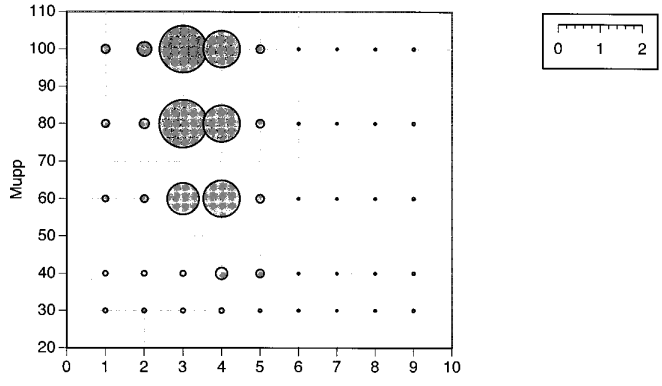

FIG. 2*c*

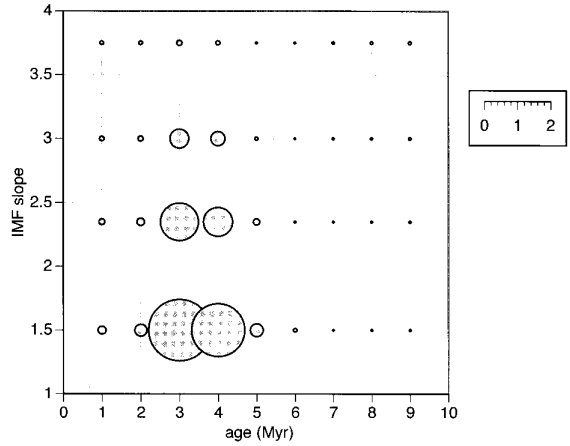

FIG. 2*d*

FIG. 2.—χ^2 parameter of the fits to the profile of C IV (*a*, *b*) and Si IV (*c*, *d*) in IRAS 0833+6517 for burst models with different M_{up} (*a*, *c*) and IMF slope (*b*, *d*). The size of the bubble is proportional to χ^2, larger size indicating a worse fit. The scale in the small boxes indicates the value of χ^2.

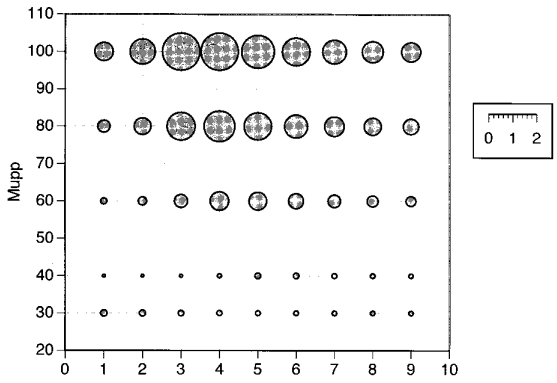

FIG. 3*a*

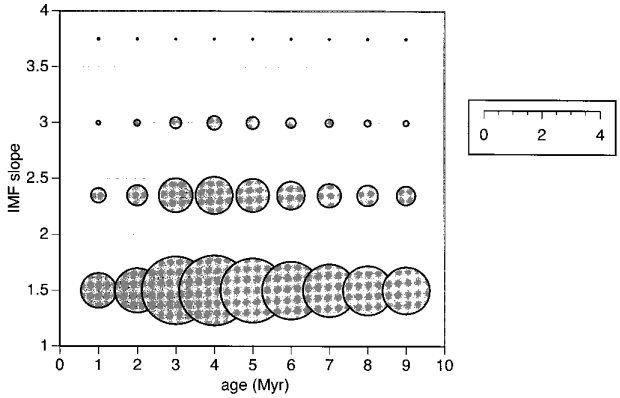

FIG. 3*b*

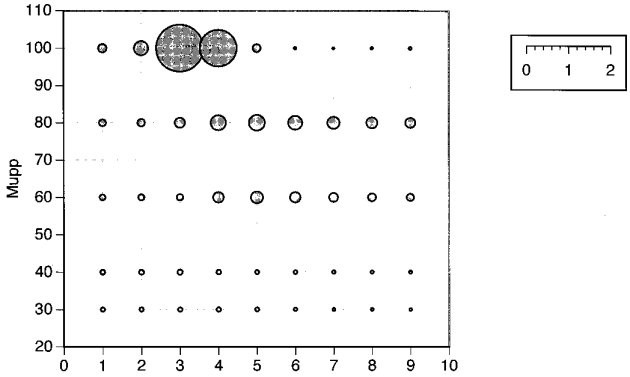

FIG. 3*c*

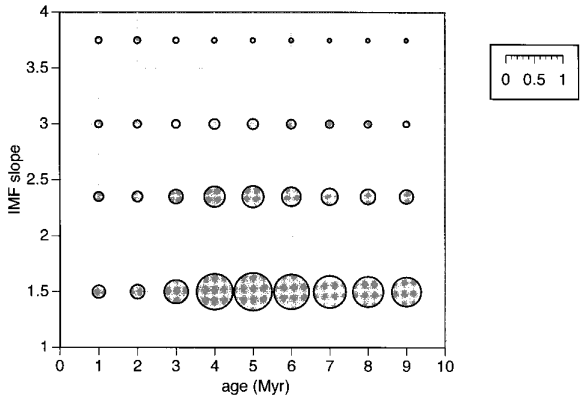

FIG. 3*d*

FIG. 3.—Same as Fig. 2, but for CSF models

contributors to this feature are O VI λ1032, 1038, Lyβ, and C IIλ 1036, 1037. The contribution of both stellar and interstellar C II must be small, since we cannot identify any line at the rest wavelength of C II (for the stellar component) or blueshifted about 2 Å because of the interstellar component (see § 5 for an explanation). We estimate that the equivalent width of the interstellar C II component is 1.3 Å. This is derived from the equivalent width of interstellar C II λ1335, assuming that these lines are on the flat part of the curve of growth, so that the ratio of the equivalent width over the wavelength is constant. Although this feature is predicted to be very broad and strong in the poststarburst phase, we can exclude all such poststarburst models because stellar C II is not clearly present (see Paper I, Figs. 7*e*–7*h*). This also means that we can exclude stellar Lyβ as the sole contributor, because the equivalent width of this line in stars hotter than B0 is less than 2 Å (Paper I). Moreover, this feature cannot be mainly the interstellar Lyβ, since an equivalent width of interstellar Lyβ of 14.4 Å implies an H I column density larger than 10^{22} cm^{-2}, which is much larger than the value derived using a normal dust-to-gas ratio and the reddening (less than 10^{21} cm^{-2}). We can also exclude the interstellar O VI as the sole contribution for the large value of the equivalent width, the broadening of the feature, and the shift with respect to the rest wavelength. Typical values of the equivalent width of the interstellar O VI detected in the coronal gas in the Galaxy are less than 0.1 Å (York 1974).

Thus, the feature seems to be mainly the product of stellar O VI + interstellar Lyβ. A direct comparison of the profile with a O VI + Lyβ + C II burst synthetic model at 6 Myr, which is one of the models compatible with the C IV and Si IV profiles, shows that the observed feature is stronger than the model, probably indicating a stronger contribution of O VI and/or interstellar Lyβ. The O VI profile of an individual O star (Fig. 6) is generally similar to the one observed. However, there are two important differences. First, the emission part of the P Cygni profile seems to be destroyed by some absorption in the galaxy, and second, the blue wing of the observed profile is broader and stronger than that in the star. We note that the blue wing of Lyα (which is detected in emission) is affected by absorption in neutral gas that is blueshifted with respect to the rest wavelength (see § 6). Figure 7 shows the velocity profile of the O VI + Lyβ feature and the Lyα wavelength region, with the rest wavelength of Lyβ and Lyα taken as zero velocity. Thus, we suggest that the excess absorption in the blue wing of the O VI profile could be produced by blueshifted interstellar Lyβ absorption with a velocity larger than 3000 km s^{-1}. If this is confirmed, an extraordinary outflow of neutral gas in this starburst has been detected.

4.1.3. *Ultraviolet Continuum Luminosity and* Hα *Equivalent Width*

From the line profile analysis, we can exclude all the burst models that require stars more massive than 40–50 $M_\odot$ to be currently present. Burst models younger than 5 Myr are excluded if $M_{up} \geq 50\ M_\odot$ or if the IMF slope is flatter than $\alpha = 3$. But any age is possible if $M_{up} \leq$ 30–40 $M_\odot$ or $\alpha \geq 3.75$. We can also exclude all CSF models if the IMF slope is flatter than $\alpha = 3$ or $M_{up} \geq 50\ M_\odot$. Now

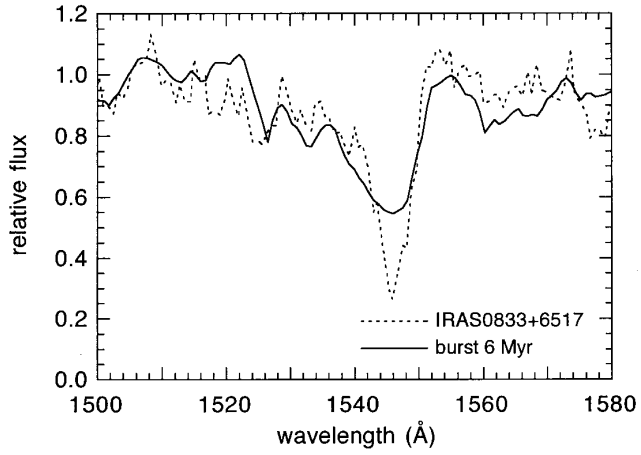

FIG. 4*a*

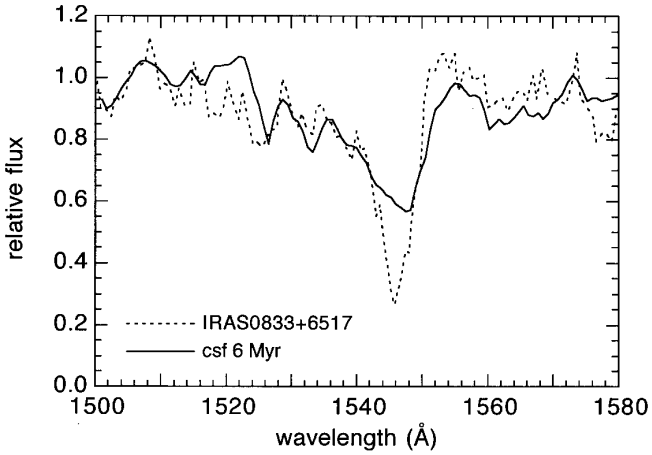

FIG. 4*b*

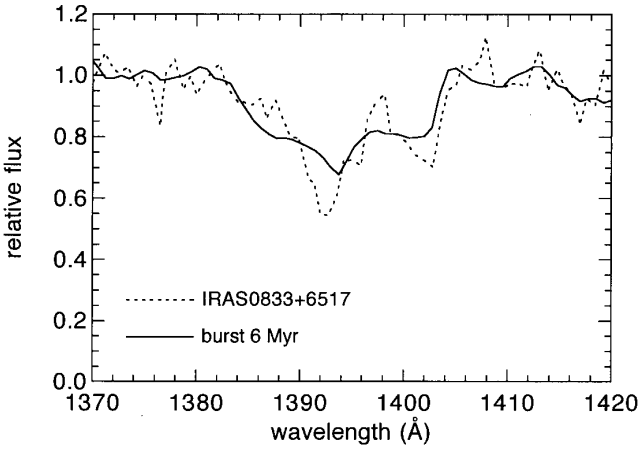

FIG. 4*c*

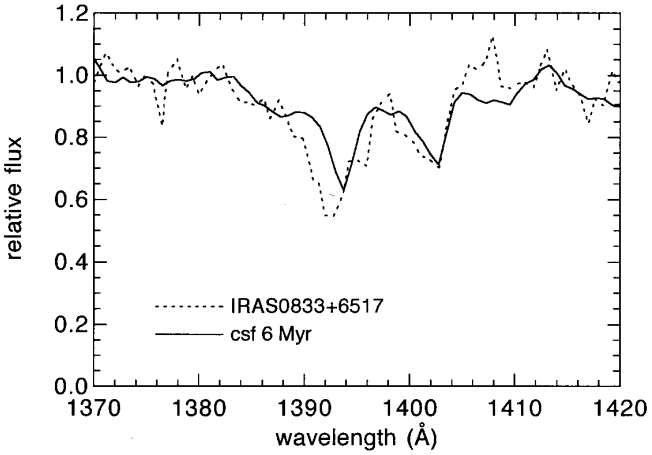

FIG. 4*d*

FIG. 4.—C IV (*a*, *b*) and Si IV (*c*, *d*) profiles of the GHRS spectrum of IRAS 0833+6517 (*dashed line*). Synthetic burst (*a*, *c*) and CSF (*b*, *d*) profiles at 6 Myr (*solid line*). The IMF slope is Salpeter, and $M_{up} = 30M_{\odot}$.

we use the UV continuum luminosity to further constrain the range of possible models.

Figure 8 shows the 6 Myr burst model with $M_{up} = 30M_{\odot}$ overplotted on the HUT spectrum dereddened by $E(B-V) = 0.17$ using the LMC law. After dereddening, and assuming a distance of 78 Mpc, the luminosity at 1500 Å is $10^{41.02}$ ergs s^{-1} Å^{-1}. This value can be used to predict the number of ionizing photons, Q, for models that are compatible with the C IV and Si IV line profiles. Note that if we use the MW extinction law and $E(B-V) = 0.4$, the luminosity at 1500 Å remains unchanged. $Q = 2.1 \times 10^{54}$ s^{-1} is derived from the Hβ flux observed by Margon et al. (1988)

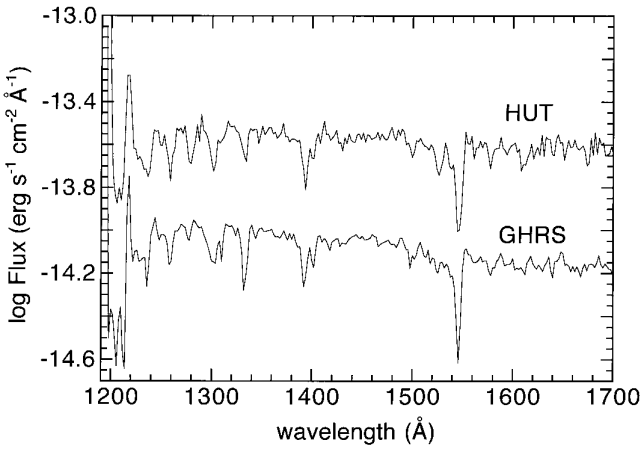

FIG. 5.—HUT and GHRS spectra of IRAS 0833+6517. The GHRS spectrum is rebinned to the resolution of the HUT spectrum.

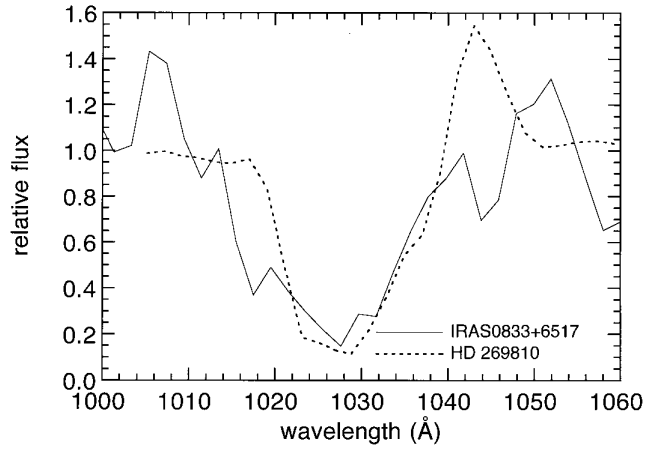

FIG. 6.—O VI + Lyβ + C II profile of IRAS 0833+6517 (*solid line*) and the LMC star HD 269810 (*dashed line*).

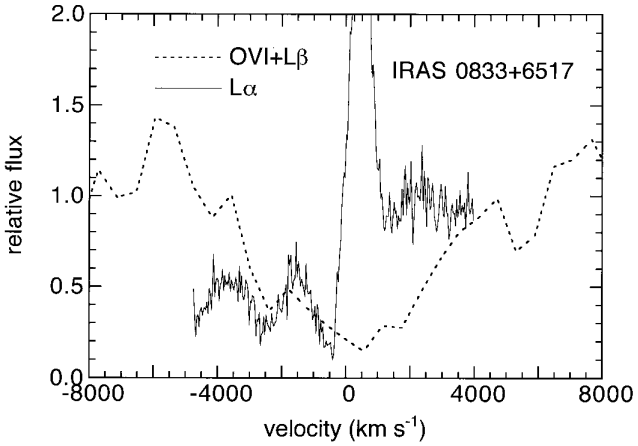

FIG. 7.—Velocity profile of O VI + Lyβ (*dashed line*) and Lyα (*solid line*). Zero velocity is the rest wavelength of Lyβ and Lyα.

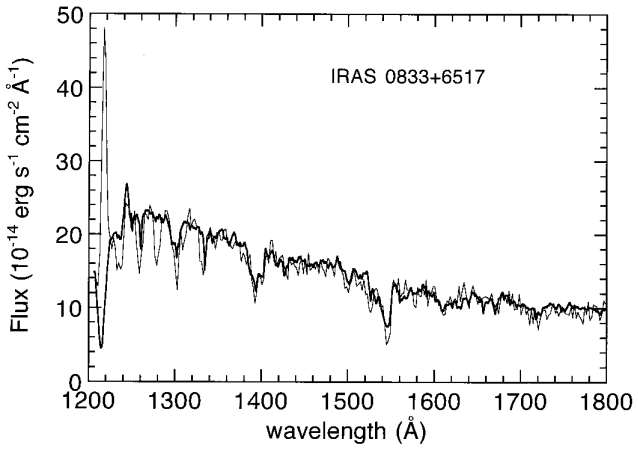

FIG. 8.—HUT spectrum of IRAS 0833+6517, dereddened by $E(B-V) = 0.17$ using the LMC law (*thin line*) and the synthetic 6 Myr–old burst model (*thick line*). The IMF slope is Salpeter, and $M_{up} = 30\ M_\odot$.

after correcting by the reddening derived from the Balmer decrement, and assuming the radiation-bounded, large optical depth case B. The best model would be one that fits the profiles of the stellar components of C IV and Si IV and also predicts a Q value equal to that derived from the recombination lines. Table 3 gives the predicted values of Q for each model. In all the cases, the models underpredict the Hβ flux. This could be because of an overestimation of the $E(B-V)$ derived from the Balmer decrement, which could come about if Hβ, which is more affected than Hα by the underlying absorption, is not corrected for this effect. Note that 6–9 Myr burst models with $M_{up} = 40\ M_\odot$ predict values of Q similar to those of models with $M_{up} = 30\ M_\odot$, but CSF models with $M_{up} = 40\ M_\odot$ predict Q values 50% larger than those of models with $M_{up} = 30\ M_\odot$. CSF models predict a star formation rate ranging from 135 $M_\odot$ yr^{-1} to 12 $M_\odot$ yr^{-1} (for CSF during 1 to 9 Myr, respectively). The star formation rate derived from the Hα flux using the expression computed by Kennicutt (1983) is 26 $M_\odot$ yr^{-1}. This rate is higher than the value of 5 $M_\odot$ yr^{-1} derived using the B magnitude of the galaxy obtained from the spectrum published by Margon et al. (1988). This indicates that the actual star formation rate is higher than the average star formation rate during the last 10^8 yr. The same conclusion is obtained if we compute the evolutionary indices proposed by Gallagher, Hunter, & Tutukov (1984), which indicate that the present rate ($\alpha_c = 5.2$) is higher than the average rate during the last 10^8 yr ($\alpha_L = 0.5$).

We can use the equivalent width of a recombination line such as Hα as an additional constraint. However, this physical parameter should be used with caution, since the equivalent width of any recombination line could be diluted by the existence of an underlying population that could contribute to the continuum at the optical wavelength but not to the ionization of the gas. Nevertheless, models that predict values for the equivalent width of Hα lower than that

TABLE 3

PREDICTED PARAMETERS FROM THE MODELS FOR IRAS 0833+6517

Model	log Q (s^{-1})	EW(Hα) (Å)	[O III] 5007/Hβ ($\phi = 10^{-2}$)	[O III] 5007/Hβ ($\phi = 10^{-3}$)	[O III] 5007/Hβ ($\phi = 10^{-4}$)	N(C II) (10^{16} cm^{-2})	N(Si II) (10^{14} cm^{-2})
Burst, $M_{up} = 30\ M_\odot$							
6 Myr.....	53.81	190	3.84	2.39	1.50	2.1	2.2
7 Myr.....	53.76	140	9.60	8.20	5.1	3.5	3.8
8 Myr.....	53.69	107	...	0.0	...	6.9	1.8
9 Myr.....	53.28	25	...	0.0	...	5.6	1.6
Burst, $M_{up} = 100\ M_\odot$							
6 Myr.....	53.88	250	...	...	...	...	...
CSF, $M_{up} = 30\ M_\odot$							
1 Myr.....	54.09	1079	1.00	0.70	0.29	3.7	1.9
2 Myr.....	54.08	1064	...	0.63	...	3.8	1.9
3 Myr.....	54.08	1045	...	0.55	...	4.1	1.9
4 Myr.....	54.06	1016	...	0.46	...	4.4	1.9
5 Myr.....	54.01	940	...	0.38	...	4.6	1.9
6 Myr.....	54.00	640	0.49	0.38	0.17	4.6	1.9
7 Myr.....	53.95	480	1.02	0.89	0.56	3.9	3.3
8 Myr.....	53.92	380	...	...	...	...	...
9 Myr.....	53.90	327	1.60	1.33	0.83	5.5	3.0
Data	54.32	118–264	...	1.8	...	>0.04	>1.5

NOTE.—Slope of the IMF is $\alpha = 2.35$. CLOUDY models are generated assuming a filling factor of $\phi = 10^{-2}$, 10^{-3}, and 10^{-4}. Column densities are derived from the models with $\phi = 10^{-3}$. The models are normalized to the dereddened observed luminosity at 1500 Å.

observed can be excluded. We estimate that the equivalent width of Hα [(Hα)] from the Margon et al. (1988) spectrum is 118 Å. Note that these observations were done with an aperture of 22″, which is similar to the HUT aperture. However, this is a lower-limit value of EW(Hα), since in addition to the effect of an underlying population, EW(Hα) may also be affected by reddening, since the stars and gas may not be affected by the same amount of dust. If we assume that the nebular light is affected by reddening derived from the Balmer decrement and that the stellar light is affected by reddening derived from the UV continuum slope, then the equivalent width of Hα after dereddening is 264 Å (assuming the $E(B-V)$ derived using the UV continuum slope and the extinction law of Kinney et al. [1994]). With this value of the equivalent width, we can only exclude burst models older than 8 Myr.

4.1.4. *The Excitation Ratio* [O III]/Hβ

Finally, we can also use the excitation ratio [O III]/Hβ to further constrain the models. This ratio depends mainly on the hardness of the ionizing spectrum, the ionization rate, and the metallicity of the gas. This means there is a dependence on the total mass and age of the starburst. We have computed photoionization models using the code CLOUDY (C90.03; Ferland 1996), taking as ionizing spectrum the spectral energy distribution of the models that fit the stellar component of C IV and Si IV, the Q value predicted for each model, a metallicity of 0.6 times solar, and a constant electron density of 100 cm^{-3}. We compute spherical models with different values of the filling factor, ϕ. A change in ϕ is equivalent to a change in the ionization parameter, U, because U is proportional to the filling factor, $U \propto (QN_e\phi^2)^{1/3}$. Table 3 gives [O III]/Hβ for $\phi = 10^{-2}$, 10^{-3}, and 10^{-4}. The models that give values of this ratio closest to the observed 1.8 (Margon et al. 1988) are the 6 Myr burst models with $\phi = 10^{-3}$ and 10^{-4} or a 9 Myr CSF model with $\phi = 10^{-2}$. Note that the variation of the excitation ratio with age reflects the changes in the spectral energy distribution (SED) with age produced by the variations of the W-R/O number. For $M_{up} = 30\ M_\odot$, the W-R/O ratio increases rapidly at ~7 Myr, the age at which the most massive stars evolve to the W-R phase; at this stage, the relative number of electrons able to excite the O^{+2} increases with respect to the number of hydrogen ionizing photons as a result of the harder SED produced by the W-R stars. We can exclude any CSF model younger than 6–7 Myr, because the predicted [O III]/Hβ is much lower than that observed (see Table 3). We can also exclude any burst model older than 6–7 Myr, because for these, Q is a factor of 4 lower than observed, and also because after this age the spectral energy distribution of the burst models is not hard enough to produce the observed high-excitation line ratio of [O III] λ5007/Hβ.

In summary, 6–7 Myr burst with $M_{up} \geq 30\ M_\odot$ or 9 Myr CSF models with $M_{up} \leq 30$–$40\ M_\odot$ are compatible with the observations. However, the weakness of the stellar UV absorption lines and the small Hα equivalent width indicate significant dilution by an underlying stellar population. The nature of this population is not clear. Most likely it is the field population of IRAS 0833+6517. If its properties are comparable to those of field star populations in the Local Group of galaxies, a relatively steep IMF is expected (Massey et al. 1995). If the observed spectrum of IRAS 0833+6517 is indeed the product of a combination of a field population and a superposed starburst, the starburst population by itself could be weighted more heavily toward massive stars than suggested by the formal IMF parameters given in Table 3.

4.2. *Mrk 1267*

4.2.1. C IV *and* Si IV *Synthesis Profiles*

The spectrum of this galaxy is noisier than that of IRAS 0833+6517, which makes the χ^2 results for C IV and Si IV much less reliable. C IV and Si IV are much weaker here than in the starburst NGC 1741, more similar to those in IRAS 0833+6517. This means that the burst is in an advanced stage of evolution, older than 5 Myr, and/or that $M_{up} \leq 40\ M_\odot$. To illustrate this, Figure 9 shows the HUT spectrum dereddened by $E(B-V) = 0.24$ using the LMC law and the 6 Myr burst model with $M_{up} = 30\ M_\odot$ (a 6 Myr burst model with $M_{up} = 100\ M_\odot$ is also consistent with the observations, since at this age stars more massive than 30 $M_\odot$ have already disappeared). Note that this model can fit the absorption section of C IV and Si IV and also the P Cygni profile of N V. Continuous star formation models with a low M_{up} are also possible.

4.2.2. O VI + Lyβ + C II *Synthesis Profile*

Figure 10 shows the absorption feature between 1015 and 1060 Å. The equivalent width is 7.6 Å. Two absorption minima are detected, one associated with C II (probably mainly interstellar), the other with Lyβ + O VI. There is good agreement between the observed profile and the 6 Myr–old burst model, except in the C II line, which is stronger in the starburst spectrum than in the model, indicating a larger contribution from the interstellar component. We also note that this feature is blueshifted about 1 Å with respect to the models. We do not find a physical interpretation for this, and attribute it to a worse wavelength calibration here than in the Si II λ1260 and C II λ1335 wavelength region, where the uncertainty in the zero-point calibration is 0.5 Å (see § 5). Thus, the absorption feature seems to indicate the presence of late O stars (O7–O9), for which the O VI stellar feature is still important.

4.2.3. *Ultraviolet Continuum Luminosity and* Hα *Equivalent Width*

After dereddening Hα by $E(B-V) = 0.55$, we derive a number of ionizing photons of $10^{53.57}$ s^{-1}. The equivalent

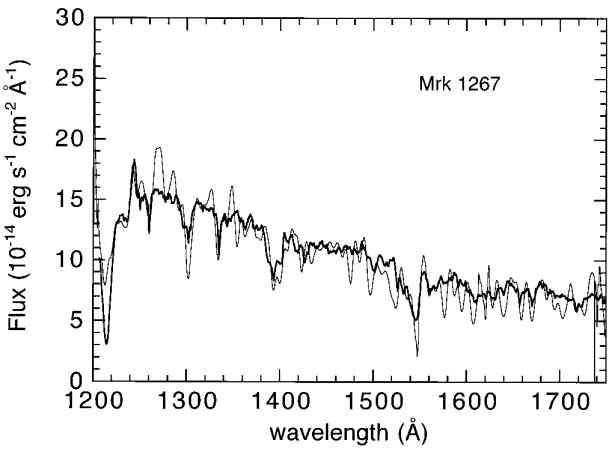

FIG. 9.—HUT spectrum of Mrk 1267, dereddened by $E(B-V) = 0.24$ using the LMC law (*thin line*) and the synthetic 6 Myr–old burst model (*thick line*).

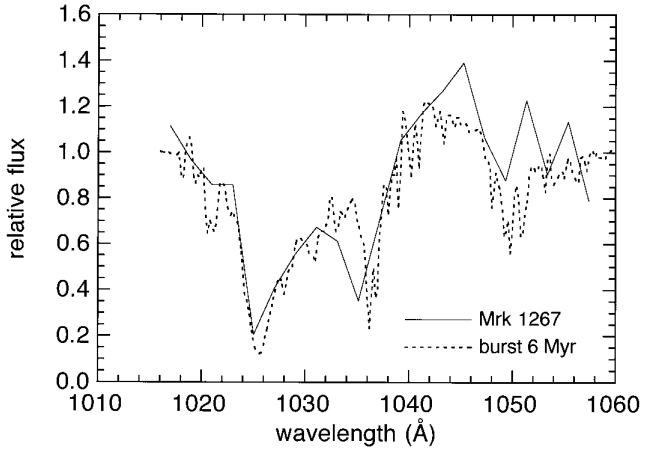

FIG. 10.—O VI + Lyβ + C II profile of Mrk 1267 (*solid line*) and the synthetic 6 Myr–old burst model (*dashed line*).

width of Hα is 49 Å (Calzetti et al. 1994), which becomes 100 Å after dereddening [we have assumed that the stellar light is affected by $E(B-V) = 0.24$ and the nebular light by $E(B-V) = 0.55$]. The luminosity of the continuum at 1500 Å is $10^{40.83}$ ergs s^{-1} Å^{-1} after dereddening by $E(B-V) = 0.24$. Scaling this luminosity to the value predicted by the models, we conclude that the CSF models are able to reproduce Q (for example, the 3 Myr CSF model with $M_{up} = 30\ M_\odot$ predicts $Q = 10^{53.49}$ s^{-1} and a star formation rate equal to 31 $M_\odot$); however, they predict values of EW(Hα) that are too large (see Table 3). As we have mentioned earlier, the EW(Hα) also could be affected by an older underlying population that contributes to the continuum but not to the ionization, making the EW(Hα) lower than the values predicted by the models. Burst models with ages between 6 and 8 Myr are able to reproduce Q and EW(Hα) (Table 4). This means that the starburst in Mrk 1267 is at an advanced stage of evolution. Again, we note the possibility of an underlying field population that may bias the derived IMF parameters toward less massive stars. The star formation rate derived using the B luminosity of the galaxy after correction for Galactic and intrinsic absorption is 2.3 $M_\odot$ yr^{-1}. This is similar to the star formation rate derived from the Hα flux, 4.5 $M_\odot$ yr^{-1}. The evolutionary indices α_c (0.9) and α_L (0.2) are very similar, indicating that the present star formation rate is not significantly higher than the average in the last 10^8 yr.

TABLE 4

PREDICTED PARAMETERS FOR MODELS THAT BEST FIT THE C IV AND Si IV PROFILES OF MRK 1267

Burst Model	log Q (s^{-1})	EW(Hα) (Å)
5 Myr, 30 $M_\odot$	53.56	540
6 Myr, 30 $M_\odot$	53.61	190
7 Myr, 30 $M_\odot$	53.57	140
8 Myr, 30 $M_\odot$	53.50	107
9 Myr, 30 $M_\odot$	53.09	25
6 Myr, 100 $M_\odot$, Burst	53.69	250
Data	53.57	49–100

NOTE.—Slope of the IMF is $\alpha = 2.35$, and the mass indicated is M_{up}. Models are normalized to the dereddened observed luminosity at 1500 Å.

4.3. *Mrk 66*

4.3.1. C IV *and* Si IV *Synthesis Profiles*

The metallicity of Mrk 66 is about one-third solar. Stars with this metallicity and lower show C IV and Si IV P Cygni profiles that are weaker than stars in the solar neighborhood (Robert et al. 1997). However, Vacca et al. (1995) have shown that the library at solar metallicity can still be applied to the 30 Doradus region, which has a metallicity of 0.3 $Z_\odot$. The spectrum of Mrk 66 does not show any clear stellar contribution in the Si IV and C IV lines, indicating a strong effect of metallicity in this starburst, or/and an advanced stage of evolution, and/or dilution by an underlying field population.

4.3.2. O VI + Lyβ + C II *Synthesis Profile*

Consistent with the weak lines of C IV and Si IV, the absorption feature between 1010 Å and 1060 Å does not show any stellar O VI. The two absorption features observed are dominated by interstellar Lyβ and C II; as with other interstellar lines (see § 5), both lines are blueshifted by about 1000 km s^{-1} with respect to the rest wavelength (taking the Lyα emission as a reference point).

4.3.3. *Ultraviolet Continuum Luminosity and* Hα *Equivalent Width*

After dereddening by $E(B-V) = 0.11$, the luminosity at 1500 Å is $10^{40.3}$ ergs s^{-1} Å^{-1}. The number of ionizing photons derived from the Hα luminosity is $10^{53.0}$ s^{-1}. Note that the $E(B-V)$ derived from the Balmer decrement is 0.0 (Calzetti et al. 1994); thus, the nebular light is not affected by reddening. The observed equivalent width of Hα is 77 Å (Calzetti et al. 1994). This value is not correcting for reddening. This small equivalent width is incompatible with all the CSF models younger than 50 Myr, assuming a Salpeter IMF slope (see Fig. 44 in Leitherer & Heckman 1995) and that the optical continuum light is not affected by an underlying population. Both the EW(Hα) and Q are compatible with burst models in the range of 7–9 Myr. Accounting for dilution would lead to starburst populations with correspondingly more massive stars. As in Mrk 1267, the star formation rate derived from the Hα flux and the B luminosity are very similar, 1.2 and 2 $M_\odot$ yr^{-1}, respectively, indicating that the current star formation rate is not higher than average.

4.4. *NGC 6090*

4.4.1. C IV *and* Si IV *Synthesis Profiles*

NGC 6090 is the most distant galaxy of the starbursts studied here, and it also has the largest metallicity (close to solar). The C IV and Si IV lines indicate a larger stellar contribution than in the previous objects, probably due to the earlier evolutionary stage of this starburst compared to the other objects, or a more powerful starburst compared to the field population. To constrain the star formation history from the C IV and Si IV profiles, we have applied the same technique used for IRAS 0833+6517; we fitted the two wavelength windows corresponding to the red and blue sides of C IV and Si IV profiles and then computed the χ^2 parameter. Figures 11 and 12 show the results for burst and CSF models, respectively. The Si IV profile is a good discriminator between burst and CSF models. This line shows a conspicuous P Cygni profile if very massive stars are present in the starburst and if the star formation process

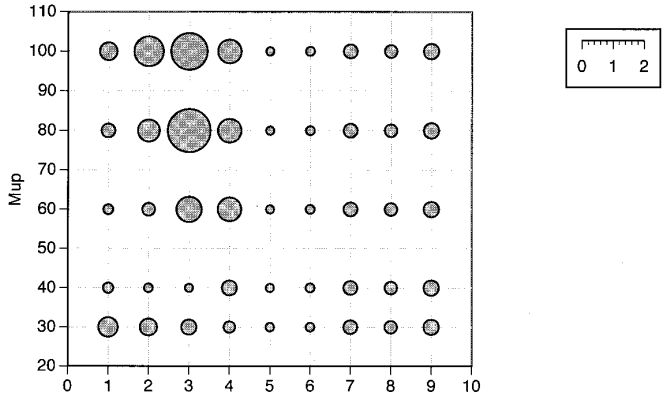

FIG. 11*a*

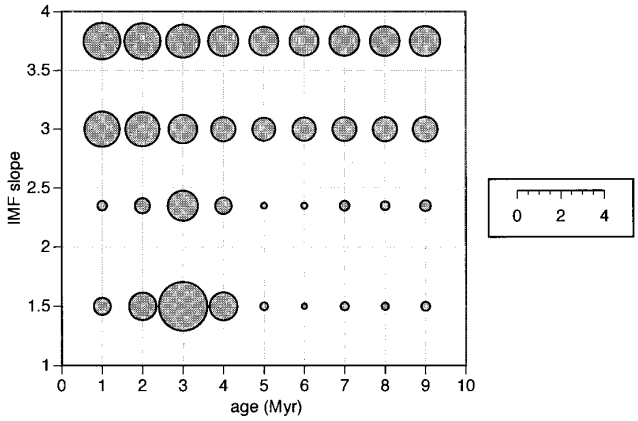

FIG. 11*b*

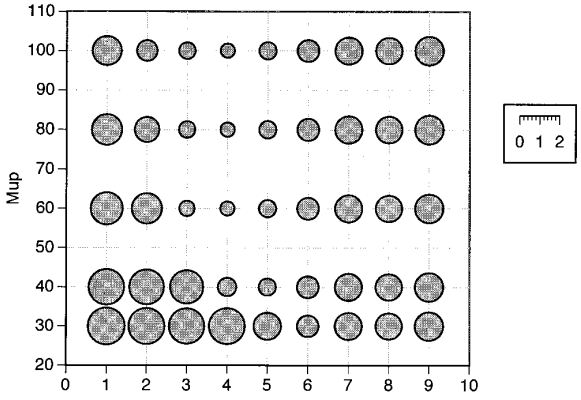

FIG. 11*c*

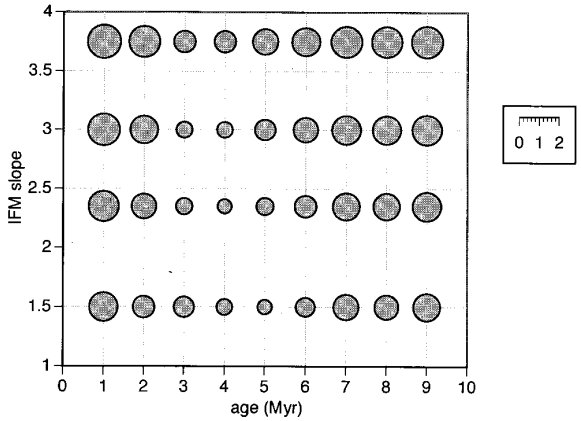

FIG. 11*d*

FIG. 11.—Same as Fig. 2, but for NGC 6090

occurs in a very short period of time. This is because the P Cygni profile is produced only by blue supergiants, which live only for a short period of time, and whose total number in a cluster is not very large compared with the total number of O stars. We can exclude the CSF models based on the fit to Si IV (Fig. 12). For burst models, the C IV fit gives a minimum age between 5 and 6 Myr and an IMF with a Salpeter exponent ($\alpha = 2.35$) or flatter ($\alpha = 1.5$), while the Si IV fit indicates an age between 3 and 5 Myr and $M_{up} \geq 60\ M_{\odot}$. Thus, we can conclude that very massive stars are present in the starburst and that star formation occurred 3–6 Myr ago in a very short period of time.

4.4.2. O VI + Lyβ + C II *Synthesis Profile*

The spectrum between 1010 and 1060 Å shows a P Cygni profile. O VI, and therefore O stars, are clearly detected. The equivalent width of the absorption profile is 10.6 Å, and the emission region has an equivalent width of 2.2 Å. Figure 13 shows the observed feature compared with the burst model and SK $-66°172$, an O4 star in the LMC. The stellar and galactic features agree rather well, except in the absorption feature at 1034 Å. This line is the interstellar C II λ1036, 1037, which is blueshifted with respect to the rest wavelength, along with the other interstellar lines (see § 5). A comparison with the 5 Myr burst model indicates that the emission is stronger in the observed profile than in the models, and also that the absorption region is broader than in the models. This is likely the result of some contribution by interstellar Lyβ blueshifted by several Å, and also a stronger contribution of stellar O VI in blue supergiants than in main-sequence stars, thus making the P Cygni profile more conspicuous than predicted by our models. Note that in our modeling we do not make a distinction by luminosity class, since in general the O VI profile does not depend much on luminosity (see Fig. 5 of Paper I). Therefore, our stellar library only distinguishes by spectral class.

4.4.3. *Ultraviolet Continuum Luminosity and* Hα *Equivalent Width*

We can exclude the CSF models from the line profile synthesis, since such models predict weaker stellar Si IV absorption than that observed. The C IV profile lets us exclude burst models with an IMF slope steeper than Salpeter. We use the predicted Q values derived from the luminosity at 1500 Å to further constrain the possible models. After dereddening by $E(B-V) = 0.22$ using the LMC law, the luminosity at 1500 Å is $10^{41.07}$ ergs s^{-1} Å^{-1}. Note that we would obtain the same luminosity if we used the MW extinction law and $E(B-V) = 0.5$. The dereddened Hα luminosity [using $E(B-V)$ from the Balmer decrement] implies that the number of ionizing photons is $Q = 10^{54.55}$ s^{-1}. This value is compatible with burst models younger than 3 Myr; however, from the line profile modeling, the best models are bursts with ages between 4 and 6 Myr. However, these models underestimate the Hα flux by a factor larger than 2 (see Table 5). Note that the HUT flux is about 30% lower than the *IUE* flux; thus, the missing radiation in the HUT aperture cannot account for the difference between the predicted and observed Balmer flux. Figure 14

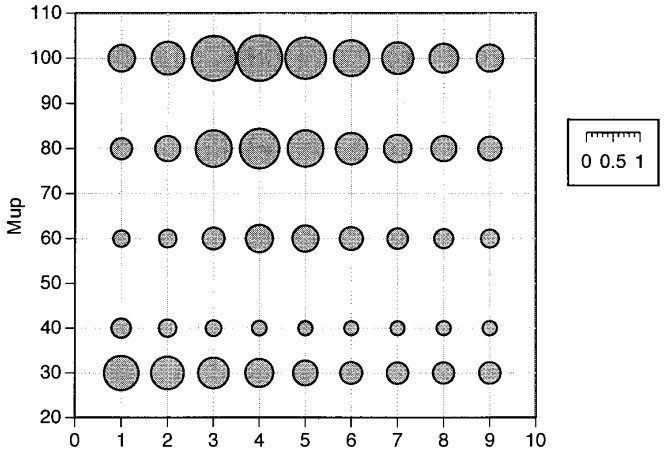

FIG. 12*a*

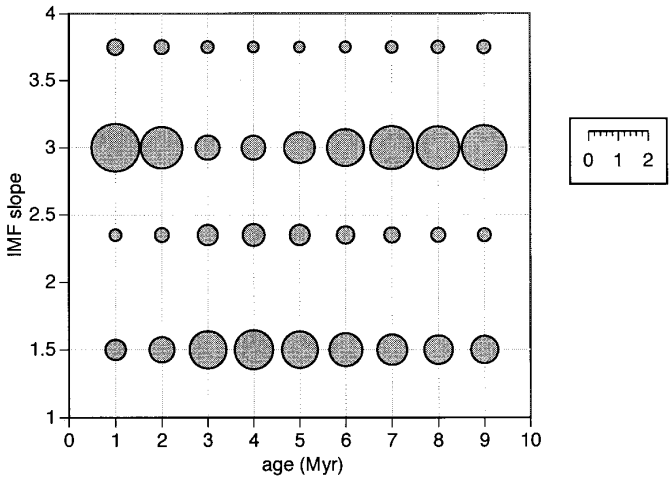

FIG. 12*b*

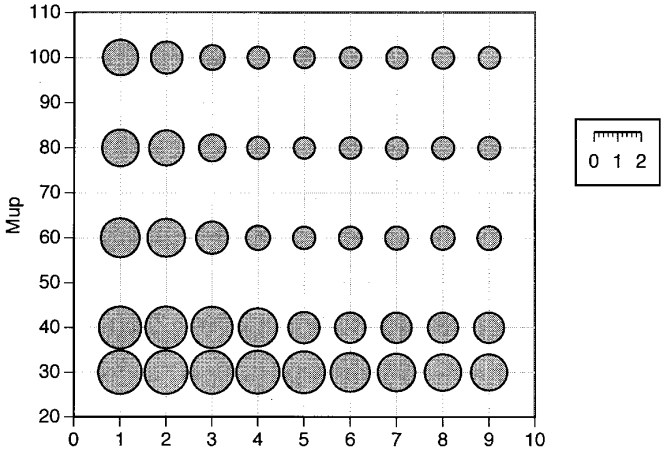

FIG. 12*c*

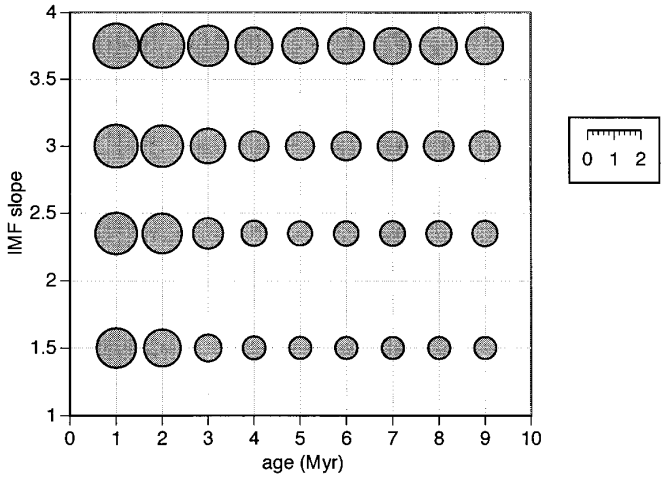

FIG. 12*d*

FIG. 12.—Same as Fig. 3, but for NGC 6090

TABLE 5

PREDICTED PARAMETERS FOR MODELS THAT BEST FIT THE C IV AND Si IV PROFILES OF NGC 6090

Model	log Q (s^{-1})	EW(Hα) (Å)	[O III]/Hβ ($\phi = 10^{-3}$)	[O III]/Hβ ($\phi = 10^{-5}$)	N(C II) (10^{16} cm^{-2})	N(Si II) (10^{14} cm^{-2})
Burst, $M_{up} = 100\ M_\odot$						
1 Myr.....	54.6	2754	2.3	0.51	0.8	0.8
2 Myr.....	54.5	2340	1.4	0.20	0.7	0.7
3 Myr.....	54.3	1510	3.6	0.98	1.1	1.0
4 Myr.....	54.2	850	3.7	1.06	1.1	1.0
5 Myr.....	54.1	390	5.0	1.15	1.0	0.95
6 Myr.....	53.9	250	4.7	1.05	1.1	1.0
7 Myr.....	53.8	140	7.5	1.63	1.5	1.3
8 Myr.....	53.7	107	0.0	0.0	0.7	0.5
Burst, $M_{up} = 30\ M_\odot$						
3 Myr.....	54.0	870	...	...	...	...
5 Myr.....	53.8	540	...	...	...	...
6 Myr.....	53.85	250	...	...	...	...
Data	54.55	157–377	...	0.75, 1.5	>0.1	>1.5

NOTE.—CLOUDY models are generated assuming a filling factor of $\phi = 10^{-3}$ and 10^{-5}. Column densities are derived from the models with $\phi = 10^{-5}$. Models are normalized to the dereddened observed luminosity at 1500 Å.

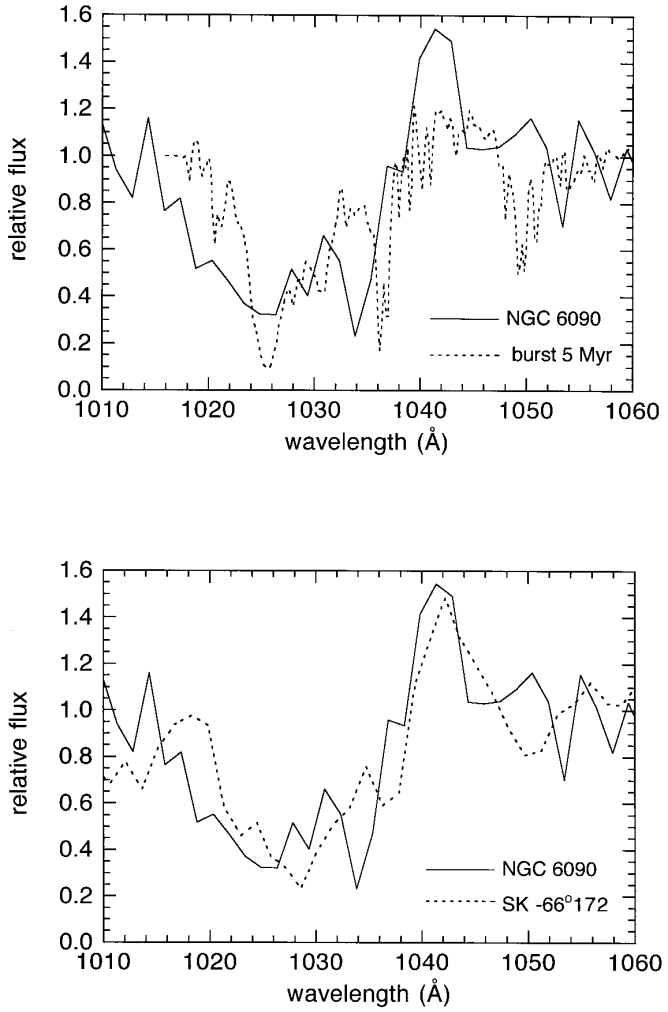

FIG. 13.—O VI + Lyβ + C II profile of NGC 6090 (*solid line*) and the spectrum of the star SK −66°172 (*bottom panel, dashed line*) and the synthetic 5 Myr burst model (*top panel, dashed line*).

shows the dereddened HUT spectrum and the 5 Myr burst model.

We use the EW(Hα) as a second constraint. The observed values before and after correcting for reddening are 157 Å and 377 Å, respectively. Burst models of ages 5 and 6 Myr are compatible with the observed value.

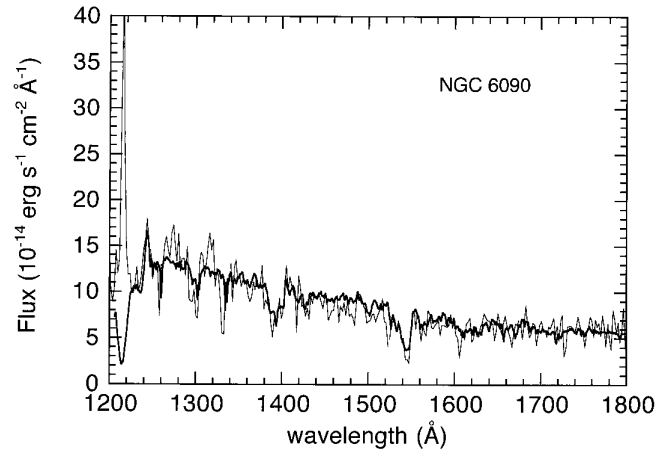

FIG. 14.—HUT spectrum of NGC 6090, dereddened by $E(B-V) = 0.22$ using the LMC law (*thin line*) and the synthetic 5 Myr–old burst model (*thick line*).

The current star formation rate in NGC 6090 derived from the Hα flux is 43 $M_\odot$ yr^{-1}, which is higher than the average star formation rate derived from the B luminosity of the galaxy, 5.6 $M_\odot$ yr^{-1}. The α-indices ($\alpha_c = 9$ and $\alpha_L = 0.5$) indicate that recent star formation is more conspicuous than in the past.

4.4.4. *The Excitation Ratio* [O III]/Hβ

Finally, we can use the predicted [O III]/Hβ ratio to constrain the models. As in the case of IRAS 0833+6517, we compute photoionization models assuming a spherical geometry, constant electron density of 100 cm^{-3}, metallicity 0.76 times solar, and Q equal to the value predicted for each model. We take as the ionizing spectra the spectral energy distributions from the models that fit the stellar component of C IV and Si IV. We have computed models with $\phi = 10^{-3}$ and 10^{-5}. Burst models with ages between 3 and 6 Myr and $\phi = 10^{-5}$ predict a ratio [O III]/Hβ close to that observed, 0.75–1.5 (Calzetti & Kinney 1992; Hartmann, Huchra, & Geller 1984). To summarize, 3–6 Myr burst models are compatible with the observations of NGC 6090.

5. THE INTERSTELLAR ABSORPTION LINES

The UV spectra of starburst galaxies are also rich in strong absorption features formed in the interstellar medium. The most important lines are Al II λ1670, Fe II λ1608, C IV λ1550, Si II λ1526, Si IV λ1400, C II λ1335, O I + Si II λ1303, Si II λ1260, Lyα, C II λ1036, O VI λ1038, 1032, and Lyβ. Some of these lines are superposed on or blended with resonance wind or photospheric absorption stellar lines, for example Si IV λ1400, C IV λ1550, C II λ1036, Lyβ, and O VI λ1032, 1038. It is also well known that the interstellar absorption lines in starbursts are stronger than the interstellar lines observed in the spectra of nearby stars. This is primarily because of the larger interstellar velocity dispersion in the starbursts. That is, in many starbursts, the stronger absorption lines are optically thick and the equivalent width of the lines is mainly related to the velocity dispersion of the gas instead of to the column density (e.g., Conti et al. 1996; Heckman & Leitherer 1997).

We first address the question of where these interstellar absorption lines are formed. To do so, we measure the radial velocity of the lines Si II λ1260, C II λ1335, and Si II λ1526 with respect to the adopted systemic velocity for each galaxy. We exclude other resonance lines, such as C IV and Si IV, because these are not pure interstellar lines and because their radial velocity in many cases can reflect a blueshift due to the stellar winds. A cursory inspection of Figures 8, 9, and 14 clearly indicates that the interstellar lines are blueshifted with respect to the systemic velocity, except in Mrk 1267.

In the case of IRAS 0833+6517, Si II λ1260 and C II λ1335 lines from the Milky Way are also detected. If we assume these lines are at a heliocentric velocity of zero, the corresponding lines in IRAS 0833+6517 are blueshifted with respect to the galaxy systemic velocity by 450 km s^{-1} and 520 km s^{-1}, respectively. Another signature of the outflowing gas in this galaxy is provided by the Lyα profile in the GHRS spectrum (see Fig. 7). Relative to the systemic velocity, the Lyα emission is redshifted by about 500 km s^{-1}. As in the well-studied case of Haro 2 (Lequeux et al. 1995), this is the result of the absorption of the blue half of

the Lyα emission line by the outflowing gas. Thus, in this galaxy the interstellar absorption lines are blueshifted by about 1000 km s^{-1} with respect to the Lyα emission line, and the galaxy systemic velocity is about halfway in between. We will discuss this point further in § 6 below.

We do not detect absorption lines from the Milky Way in the other three starbursts. This is owing to a combination of a worse S/N and a lower resolution in the HUT spectra than in the GHRS spectrum, and the equivalent width of the lines. Note that the MW C II λ1335 is resolved from O I + Si II λ1303 in the GHRS spectrum but not in the HUT spectrum. Since we do not know accurately the location of the centroid of the UV light within the HUT aperture, the true zero point in the HUT wavelength scale (in the starburst rest frame) is ill determined. However, both Mrk 66 and NGC 6090 have Lyα in emission. In these two galaxies, the Si II λ1260, C II λ1335, and Si II λ1526 lines are blueshifted with respect to the Lyα emission line by about 760 km s^{-1} and 480 km s^{-1}, respectively. In view of the above results for IRAS 0833+6517, these blueshifts imply high-velocity outflows of gas, of several hundred km s^{-1}. Mrk 1267 has no Lyα emission, and thus we cannot determine if there is an outflow. We cannot estimate the spatial scale associated with this gas, but it cannot be produced in isolated clouds, since ISM lines cover about 50% of the UV light (Fig. 15). Thus, this high-velocity gas probably represents a Galactic-scale outflow.

Another indicator of the large-scale motions of the interstellar gas in these starbursts is the broadening of the interstellar lines. In the GHRS spectrum of IRAS 0833+6517, the Si II λ1260 and C II λ1334 lines appear to be asymmetric, and they can be fitted by two components. One component is unresolved (instrumental resolution about 2.3 Å FWHM), centered on 1261.0 $\pm$ 0.9 Å, and has a FWHM of 2.9 $\pm$ 0.9. The other, which is the dominant contributor to the total equivalent width, is centered on 1258.4 $\pm$ 0.7 and has a FWHM of 3.8 $\pm$ 1.0 Å (corresponding to an intrinsic FWHM of about 700 $\pm$ 250 km s^{-1}; see Fig. 15*a*). C II λ1335 can also be fitted by two components. One is unresolved at the rest wavelength, and the other is blueshifted by 2.6 $\pm$ 0.2 Å, with a FWHM of 5.0 $\pm$ 0.6 Å (corresponding to an intrinsic FWHM of about 1000 $\pm$ 150 km s^{-1}; see Fig. 15*b*). The HUT spectrum does not have sufficient spectral resolution, and only one Gaussian is sufficient to fit Si II λ1260 with a FWHM of 7.0 $\pm$ 2.2 Å. Taking the FWHM of the MW C II λ1335 as the instrumental resolution, the intrinsic FWHM of Si II λ1260 derived from the HUT spectrum is 1060 $\pm$ 500 km s^{-1}, which is in agreement with the value obtained with the GHRS spectrum. In the spectra of the other three starbursts, C II λ1335 has a FWHM of 6.1 $\pm$ 2.5 Å, 5.2 $\pm$ 1.2 Å, and 5.8 $\pm$ 2.0 Å for NGC 6090, Mrk 1267, and Mrk 66, respectively. As we do not know the HUT point spread function of this line, we cannot make a reliable estimate of the intrinsic FWHM of the absorption lines in these three starbursts.

More evidence for large-scale motions of the interstellar gas comes from the equivalent width of the metallic interstellar lines. These are optically thick, and they are in the flat part of the curve of growth. This means that the equivalent width of these lines is not proportional to the column density of the gas, as would be the case if they were in the linear part of the curve of growth. Instead, the equivalent width is determined by the velocity dispersion of the gas. We can show that in fact the lines are saturated, taking for example Si II λ1260 and Si II λ1527. If these were optically thin, the equivalent width of Si II λ1527 would be about three times lower than that of Si II λ1260. However, the observed ratio is larger than $\frac{1}{3}$ (see Table 6). Therefore, an equivalent width of about 2–3 Å implies a velocity dispersion larger than 200–300 km s^{-1} (FWHM = 470–700 km s^{-1}). This may indicate that several unresolved velocity components are observed. However, we can estimate the minimum Si II and C II column densities by using the equivalent width of the lines Si II λ1527 and C II λ1334, assuming that they are in the linear part of the curve of growth. This gives minimum values that are several times 10^{14} cm^{-2} for each ion.

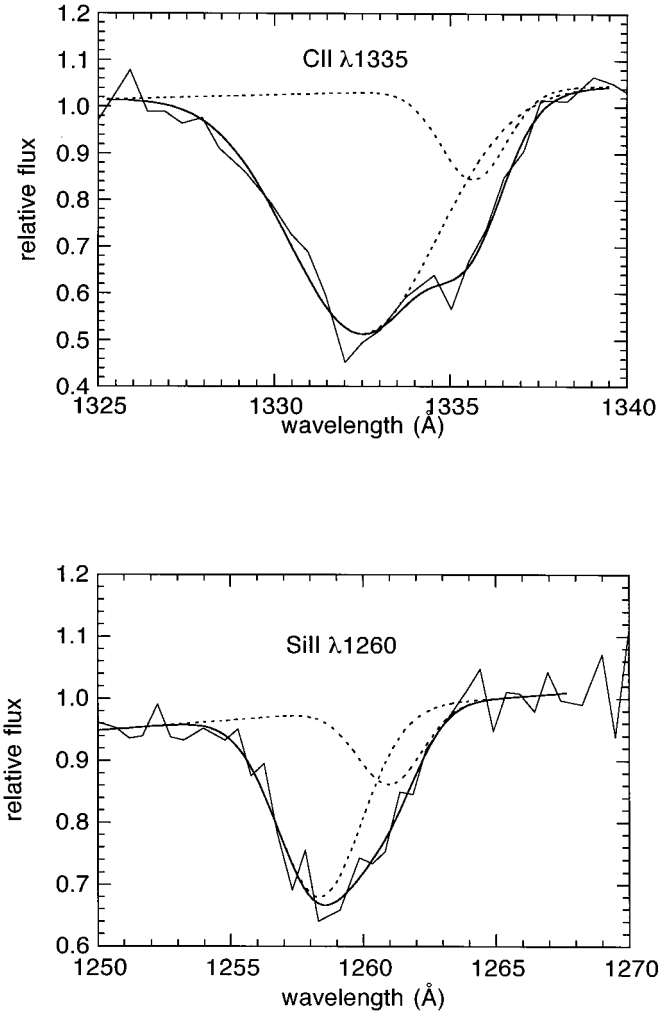

FIG. 15.—GHRS spectrum of IRAS 0833+6517 (*thin line*), showing Si II λ1260 (*bottom panel*) and C II λ1335 (*top panel*), and the two Gaussian best-fitting profiles found (*thick line*). Dashed lines are the two individual components.

Where can the Si II and C II lines be formed? The ionization potentials of these ions (8.1 eV for Si II and 11.3 eV for C II) are smaller than that of hydrogen; thus, they can be formed in an outflowing neutral or ionized medium. In § 6 we will show clear evidence for the existence of a neutral medium that is flowing away from the Lyα absorption line, at least in IRAS 0833+6517. However, we will see that the derived column densities of C II and Si II are compatible with their formation in the H II region around the starburst. We have computed photoionization models using the code CLOUDY (Ferland 1996) to determine the column den-

TABLE 6

EQUIVALENT WIDTH (Å) OF THE STRONGEST INTERSTELLAR LINES

Line	IRAS 0833+1567 (HUT)	IRAS 0833+1567 (GHRS)	Mrk 1267	Mrk 1267	NGC 6090
Si III λ1206	...	...	...	...	2.1
Si II λ1260	2.1	1.7	1.7	1.8	2.4
O I + Si II λ1303.....	2.9	3.5	4.0	4.1	4.5
C II λ1335	1.7	2.8	1.8	1.9	3.8
Si II λ1527	1.4	1.0	2.5	...	2.0
Fe II λ1608	...	...	2.4	...	3.0
Al II λ1670.....	...	...	2.0	...	...

sities of C II and Si II, taking as inputs the SED from the starburst models listed in Tables 3 and 5 and the number of ionizing photons derived from L_{1500}, and assuming a spherical geometry, a constant electron density of 100 cm^{-3}, a filling factor of 0.01, 0.001, and 0.0001, and the appropriate metallicities for IRAS 0833+6517 and NGC 6090. We also assume that Si is depleted with respect to the solar value. Therefore, we use a gas-phase Si abundance of 4×10^{-4}, which is the typical value of the interstellar medium in the Milky Way. The column densities computed have values of several times 10^{16} cm^{-2} for C II and several times 10^{14} cm^{-2} for Si II (if we assume that the Si is not depleted, the column density of Si II would be 1 order of magnitude larger than this). Models with lower values of the electron density (1 cm^{-3}) predict similar values of the column densities. Within a factor of 2–3, these values do not depend on the starburst model assumed. These values are larger than the lower limits derived from the equivalent width of the lines, indicating that these ions can be formed in an ionized medium.

6. THE Lyα EMISSION

Lyα emission can in principle be produced by recombination of hydrogen photoionized by O and B stars. The stellar clusters in starburst galaxies provide sufficient ionizing radiation to produce a large Lyα flux. However, galaxies observed with *IUE* show Lyα emission weaker than predicted by recombination theory (Meier & Terlevich 1981; Hartmann et al. 1984, 1988; Terlevich et al. 1993), and an anticorrelation between the Lyα/Hβ ratio and the metallicity is found. One possible interpretation is that Lyα photons are attenuated by dust as a result of multiple resonant scattering by hydrogen atoms that increase the path length of the Lyα photons and thus the probability that Lyα photons will be absorbed by dust. However, other authors (Calzetti & Kinney 1992; Valls-Gabaud 1993) have shown that some galaxies have a Lyα/Hβ ratio consistent with simple recombination theory if the ratio is corrected for reddening using the appropriate extinction law for the metallicity of the galaxy, and if the Hβ flux is obtained with an aperture similar to that used for the *IUE* data. This result contrasts with that of Kunth et al. (1994) for IZw 18, where no Lyα emission was detected, even though the metallicity and dust in this galaxy are very low. A few more galaxies observed with *HST* show the same behavior (Kunth et al. 1997). Furthermore, several galaxies have been detected whose Lyα emission line shows an asymmetric profile, with the peak emission redshifted with respect to the systemic velocity (Lequeux et al. 1995; Kunth et al. 1997). The explanation is that the neutral gas responsible for the absorption is blueshifted with respect to the systemic velocity, as a result of which only Lyα photons in the red wing can escape. This suggests that the amount of neutral gas and dust are not the only determining factors for Lyα emission, but that the velocity structure of the gas also matters. A similar conclusion was reached by Giavalisco, Koratkar, & Calzetti (1996) for a sample of galaxies observed with *IUE*. They found no good correlation between the equivalent width of Lyα and the reddening or metallicity, and interpreted this as evidence that the interstellar medium in these galaxies is highly inhomogeneous and that the escape of Lyα photons is determined by the geometry of the interstellar medium.

In three of the galaxies observed by us, Lyα is detected in emission. The Lyα/Hβ dereddened using the Balmer decrement is shown in Table 7. Also shown are the equivalent width of Lyα and the dereddened values, assuming that the gas is affected by the reddening derived from the Balmer decrement and the continuum by the reddening derived from the UV slope. The dereddened values in IRAS 0833+6517 and NGC 6090 are very close to the values predicted for bursts younger than 6 Myr (Valls-Gabaud 1993; Charlot & Fall, 1993). These ages are in agreement with values derived from the synthesized absorption line profiles. However, in Mrk 66 the Lyα emission line equivalent width is quite low, and the line is detected only in absorption. One possible explanation, according to those models, is that these galaxies are in a poststarburst phase. However, this disagrees with our absorption profile analysis and also with the observed strength of the Balmer emission lines.

After correcting for extinction, the Lyα/Hβ ratio in IRAS 0833+6517 and NGC 6090 is close to the recombination value (~33; Ferland & Osterbrock 1985). In Mrk 66 this ratio is much lower. One possible explanation is that the starburst is surrounded by an H I envelope, and the Lyman photons are destroyed by absorption by dust after multiple scattering with the H I atoms, because the dust optical depth is relatively small in Mrk 66 (this is our lowest metallicity starburst) and the number of ionizing photons derived from the Hβ flux is large enough. However, due to the proximity of the geocoronal Lyα and the poor spectral resolution in the HUT spectrum, we did not find any clear evidence of absorption in this object (although there is a hint of asymmetry in the Lyα profile) that could be interpreted as being due to absorption by neutral outflowing gas (see Lequeux et al. 1995). However, we do find evidence for an outflow in Mrk 66 from the Si II λ1260 and C II λ1335 lines as compared to Lyα (see § 5).

The GHRS spectrum of IRAS 0833+6517 (Fig. 16*a*) sheds more light on this issue. The peak of the Lyα line is redshifted with respect to the systemic velocity, the profile

TABLE 7

EQUIVALENT WIDTH OF Lyα (Å) AND THE Lyα/Hβ RATIO

Name	EW(Lyα)	EW($Ly\alpha_{redd}$)	Lyα/Hβ	$Ly\alpha/H\beta_{redd}$
IRAS 0833+6517 (HUT)	8.1–10.2	180–226	0.84–0.99	17.3–20.4
IRAS 0833+6517 (GHRS).....	7.1	158	0.21	4.3
Mrk 1267	−11.5	...	...	...
Mrk 66	8.2–13.8	1.76–2.86	1.76–2.86	1.76–2.86
NGC 6090	8.4–10.0	272–323	0.55–0.74	17.9–24.6

NOTE.—The range of values indicates the uncertainties in the measurements.

looks asymmetric, and deep Lyα absorption is detected blueshifted with respect to the emission line. Another absorption feature is centered on 1205 Å. We attribute this feature to interstellar Si III λ1206.5 blueshifted with respect to the systemic velocity, in agreement with the other low-ionization lines (see § 5). We have performed a multiple-component fit to the observed absorption features using theoretical Voigt profiles produced with the XVOIGT software package (Mar & Bailey 1995). We assume that as with the other interstellar lines, the Lyα absorption line is blueshifted by about 2 Å with respect to the rest wavelength,

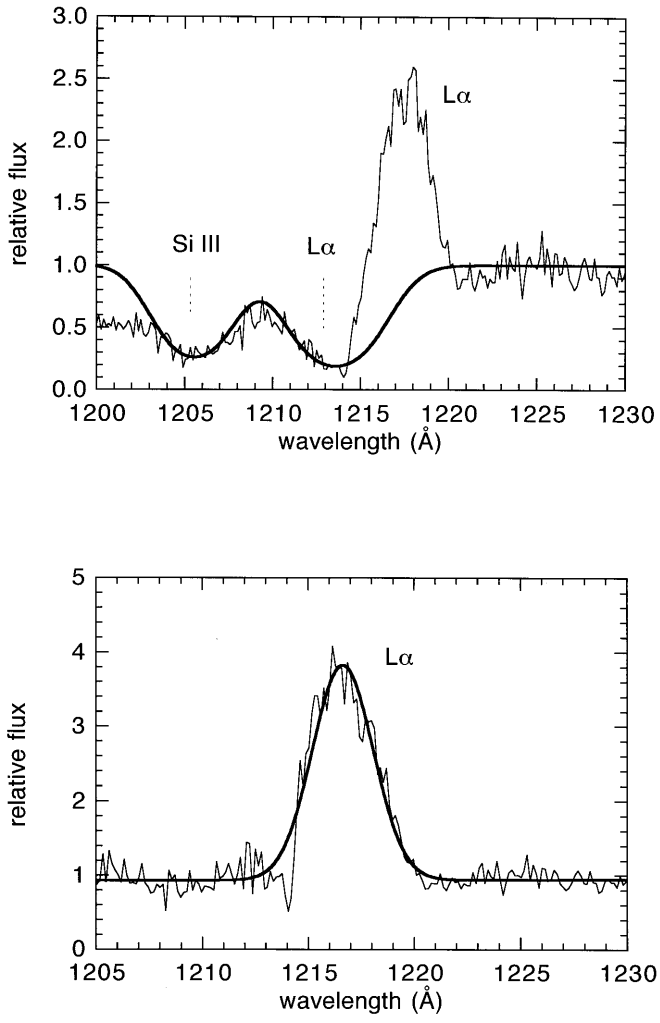

FIG. 16.—*Top panel*: Region around Lyα of the GHRS spectrum of IRAS 0833+6517 (*thin line*). Solid line is the best fit of the Voigt profiles of the Lyα and Si III λ1206.5 absorption lines. *Bottom panel*: Profile of the Lyα emission line after dividing the observed spectrum by the absorption Voigt profile fitted (*thin line*). Solid line is the best Gaussian fit found.

and we assume that the blue part of the line is not affected by Lyα emission. We also assume that the blue wing of Si III is affected by another absorption feature seen close to the geocoronal Lyα. The results of the fitting (Fig. 16*a*) give *b* parameters (corrected for the instrumental resolution) of 530 km s^{-1} and 630 km s^{-1} for Si III and Lyα, respectively. The *b* parameters indicate an interstellar velocity dispersion (FWHM = 875 km s^{-1} and 1000 km s^{-1} for Si III and Lyα, respectively) similar to the values derived from the FWHM of Si II λ1260 and C II λ1335. Again, we found evidence for large-scale motions of the interstellar gas in this galaxy. Clearly, these large values of *b* may be the result of the presence of multiple velocity components.

Next, we consider how much of the Lyα emission is affected by the absorption component, and thus whether in this starburst the velocity structure of the neutral H I gas or the abundance of dust is the determining factor for the escape of Lyα photons. The normalized observed profile was divided by the fitted Voigt profile, and the resulting profile (Fig. 16*b*) was fitted by a Gaussian emission line. The emission-line flux of the Gaussian after correction for the reddening derived from the Balmer decrement is 9.8×10^{-12} ergs s^{-1} cm^{-2}, which is 50% larger than before correction for the absorption. The GHRS aperture does not include all the Lyman photons, and the flux measured in the HUT aperture is a factor of 4 larger than that in the GHRS aperture. Therefore, we estimate that the true Lyman flux is about 4×10^{-11} ergs s^{-1} cm^{-2}, implying a Lyα/Hβ ratio of 26.6, very close to the case B recombination ratio.

The conclusion is that in IRAS 0833+6517, the velocity structure of the neutral gas and the scattering by H I atoms are not the sole determining factors for the escape of the Lyman photons, since the correction factor to the Lyα/Hβ ratio from extinction is larger than from the absorption of the neutral gas. However, these could be determining factors in low-metallicity objects where the dust-to-gas ratio is low.

7. IMPLICATIONS

7.1. *The* Lyα *Line*

One of the techniques used to look for primeval galaxies is to search for Lyα emitters; however, few strong Lyα sources have been found at high redshift, with the exception of QSOs. It has been suggested that Lyα photons are obscured by multiple resonant scattering with H I atoms, thereby increasing the optical depth across the ISM and thus the probability for absorption by dust (Neufeld 1990). This means that the Lyα emission search technique is not always a good tool for detecting candidate star-forming galaxies at high redshift (Hartmann et al. 1984). However, other studies suggest that the weakness of the Lyα emission in nearby starburst galaxies is due more to extinction than

to resonant scattering, making the technique appropriate, since the extinction in primeval galaxies should be smaller (Calzetti & Kinney 1992; Valls-Gabaud 1993). Our study does not unambiguously support either of these suggestions. For two galaxies with larger metallicity and larger Balmer decrement reddening, IRAS 0833+6517 and NGC 6090, the determining factor for Lyα emission is obscuration by normal dust extinction. The velocity structure of the H I gas and the scattering it produces seems to be only a secondary effect. However, for more metal-deficient starbursts, the normal extinction is not so important, and the H I column density and the geometrical distribution of the neutral gas and dust seem to be more important factors. In addition, the mass of the starburst and its age also seem to play some role (at least in Mrk 1267, where Lyα is purely in absorption). Bursts that are not very massive and that are in a very evolved state, in combination with large amounts of H I, will preferentially show Lyα in absorption. All these considerations indicate that the Lyα emission technique is not a straightforward tool for searching for primeval galaxies, owing to the difficulty of interpreting the Lyα emission line in terms of the rate of star formation (Charlot & Fall 1993).

A second point is related to the profile of the Lyα emission line detected in IRAS 0833+6517. This line is asymmetric, with the peak emission redshifted with respect to the systemic velocity and a deep absorption in the blue wing of the line. Evidence of the asymmetry of this line is also present in the other starbursts, but better spectral resolution, comparable to that of the GHRS spectrum, is needed to confirm this suggestion. In the three galaxies where Lyα is detected in emission, the interstellar lines are blueshifted by several hundred of km s^{-1} with respect to the systemic velocities. This means that the asymmetric Lyα line profile is a consequence of the interstellar gas outflow that absorbs the Lyα blue wing via neutral H I gas. Such outflows are undoubtedly a consequence of the star formation activity in these starbursts.

It is interesting to note that a Lyα profile similar to that seen in IRAS 0833+6517 has been detected in a candidate protogalaxy at a redshift of 3.150 (Djorgovski et al. 1996). In this galaxy, the asymmetry of the line is interpreted as consequence of the line photons passing through lines of sight that intersect the differential rotating disk of the galaxy. The profile of the line is then used to derive the dynamical mass of the galaxy. Our results suggest an alternative explanation, namely, that the profile may be the consequence of an outflow of the interstellar gas. Thus, Lyα should be used with care for mass estimates of high-redshift galaxies.

7.2. *The Dynamics of the ISM in Starbursts*

Most of the interstellar lines detected in the spectra of these starbursts are saturated. This means that the equivalent width of the lines is more representative of the velocity dispersion than of the column density. The equivalent widths indicate a large velocity dispersion. More direct evidence comes from the broadening of the Si II λ1260 and C II λ1335 lines in IRAS 0833+6517. These lines are resolved into two components, one unresolved at the rest wavelength, and the other blueshifted by several hundred km s^{-1}, having intrinsic FWHM of 700 ± 250 km s^{-1} and 1000 ± 150 km s^{-1}, respectively. This broadening is a clear indication of the large-scale motions of the interstellar gas in this starburst. This means that the kinematics of the warm ionized interstellar medium is driven more by the dynamical consequences of the violent star formation process ongoing in these galaxies than by their gravitational potential. The implication is that similar processes can occur in high-redshift galaxies. In this case, any determination of the dynamical mass of the galaxy through the velocity dispersion derived from the interstellar absorption lines would be incorrect. A similar conclusion was reached by Heckman & Leitherer (1997) from the GHRS spectrum of the nearby dwarf starburst galaxy NGC 1705.

7.3. *The Escape of UV and Ionizing Radiation*

In a previous paper (Leitherer et al. 1995a), we found that the luminosity of the burst at 900 Å is proportional to the number of Lyman continuum photons for very different IMF and star formation histories: $\log (Q_{\rm Lyc}/L_{900}) = 13.28 \pm 0.16$ (photons Å erg^{-1}) for CSF and 13.07 ± 0.50 (photons Å erg^{-1}) for an instantaneous burst. Using published Hα fluxes, corrected by the reddening derived from the Balmer decrement, Leitherer et al. (1995a) obtained the ratio of the recombinations to the luminosity at 900 Å. For the four starbursts, the observed values of this ratio are larger than the predicted theoretical value by almost 2 orders of magnitude, implying that only a few percent of the ionizing photons escape from these galaxies (but see Hurwitz et al. [1997] for some caveats). If we now correct the upper limit of the flux at 900 Å by the extinction derived from the UV slope, we obtain logarithmic ratios of 14.34, 13.22, 13.55, and 13.98 (photons Å erg^{-1}) for IRAS 0833+6517, Mrk 1267, Mrk 66, and NGC 6090, respectively. With the exception of Mrk 1267, these values are still lower than the theoretical ratio derived from the models. This implies that dust alone is not responsible for the low value of L_{900}, and absorption by gas in the galaxies and their halos may be responsible for the low fraction of photons escaping. This indicates that the fraction of ionizing photons that can escape from these galaxies is very small, and that young primeval galaxies are not likely to provide the Lyman continuum photons for the ionization of the early universe.

8. SUMMARY AND CONCLUSIONS

The present work is a continuation of the study presented by Leitherer et al. (1995a). Four starburst galaxies were observed by HUT from 820 to 1840 Å with a moderate resolution ($R = 400$ at 1200 Å). The galaxies selected are affected by very little Galactic extinction, and they show strong Hα emission, indicating a large supply of ionizing photons. The measurement of the Lyman continuum flux suggests that only a small fraction of the ionizing photons escape from these galaxies. This implies that young galaxies may not provide enough photons for the ionization of the early universe. Similar conclusions have been reported by Deharveng et al. (1997) and Hurwitz et al. (1997).

In this paper, we analyze the HUT spectra of the starbursts galaxies IRAS 0833+6517, Mrk 1267, Mrk 66, and NGC 6090 in order to constrain the stellar population and the kinematics of the interstellar medium. GHRS data for IRAS 0833+6517 are also presented. We use an analysis of the stellar component of the UV absorption lines Si IV, C IV, and O VI + Lyβ + C II to study the star formation history. The profiles of these lines are predicted by evolutionary synthesis models. These models are based on stellar libraries built with O and B stars. From the line profile analysis

and the absolute flux at 1500 Å, we conclude that O stars are present in these starbursts. The stellar components of Si IV, C IV, and O VI are weaker in IRAS 0833+6517 and Mrk 1267 than in NGC 6090. This indicates that (1) the bursts are more evolved in IRAS 0833+6517 and Mrk 1267 than in NGC 6090, or (2) NGC 6090 has more massive stars, or (3) the lines are diluted by an old population. The latter suggestion becomes even more plausible if we compare NGC 6090 with the Wolf-Rayet galaxy NGC 1741 (Conti et al. 1996). NGC 1741 is dominated by a starburst, just like NGC 6090. In both cases, the UV spectra show strong stellar P Cygni profiles.

The spectra of these starbursts are rich in interstellar absorption lines. In IRAS 0833+6517, Mrk 66, and NGC 6090 the lines are blueshifted by several hundred km s^{-1} with respect to the systemic velocity or with respect to Lyα detected in emission. These outflows might be triggered by the starburst activity. This situation differs from other local starbursts (Conti et al. 1996; Leitherer et al. 1996), in which no outflows have been detected in the UV absorption lines. Other evidence for large-scale motions of the interstellar gas comes from the broadening of the interstellar lines in IRAS 0833+6517. For the other three galaxies, it comes from the large value of the equivalent width of the interstellar absorption lines.

Lyα in emission was detected in IRAS 0833+6517, Mrk 66, and NGC 6090. The dereddened Lyα/Hβ ratio is close to the recombination value in IRAS 0833+6517 and NGC 6090, but much smaller in Mrk 66. An analysis of the absorption component of Lyα in IRAS 0833+6517 indicates that even though the velocity structure of the neutral H I gas plays an important role, it is not the sole determining factor for the escape of Lyα photons. This result suggests that in galaxies with relatively high metallicity and thus dust abundance, such as NGC 6090 and IRAS 0833+6517, the velocity structure of the neutral gas and the scattering by H I atoms are not solely responsible for the escape of the Lyman photons. However, in low-metallicity objects where the extinction is low, it could be the primary factor.

This work is dedicated to the memory of my son, who was with me (R. G. D.) all the time during the preparation of this work but did not have the chance to see the sunlight. We are very grateful to David Mar for kindly providing his XVOIGT software package, to Enrique Pérez and Danielle Alloin for many stimulating discussions and helpful suggestions, and to Gary Ferland for CLOUDY. We thanks the referee, John Gallagher, for the very detailed report that helped to improve this work. Support for the Astro-2 Guest Investigator program was provided by NASA through grant NAG 8-1075 from NASA/Marshall and by NASA grant GO-5954.01-94A from the Space Telescope Science Institute, operated by the Association of Universities for Research in Astronomy, Inc., under NAS contract NAS 5-26555.

REFERENCES

Calzetti, D., & Kinney, A. L. 1992, ApJ, 399, L39
Calzetti, D., Kinney, A. L., & Storchi-Bergmann, T. 1994, ApJ, 429, 582
Charlot, S., & Fall, S. M. 1993, ApJ, 415, 580
Conti, P. S., Leitherer, C., & Vacca, W. D. 1996, ApJ, 461, L87
Davidsen, A. F., et al. 1992, ApJ, 392, 264
Deharveng, J.-M., Faisse, S., Milliard, B., & Le Brun, V. 1997, A&A, in press
Djorgovski, S. 1992, in ASP Conf. Ser. 24, Cosmology and Large-Scale Structure in the Universe, ed. R. de Carvalho (San Francisco: ASP), 73
Djorgovski, S., Pahre, M. A., Bechtold, J., & Elston, R. 1996, Nature, 382, 18
Ebbels, T. M. D., Le Borgne, J.-F., Pello, R., Ellis, R. S., Kneib, J.-P., Smail, I., & Sanahuja, B. 1996, MNRAS, 281, L75
Ellingson, E., Yee, H. K. C., Bechtold, J., & Elston, R. 1996, ApJ, 466, L71
Fanelli, M., O'Connell, R., & Thuan, T. 1988, ApJ, 334, 665
Ferland, G. J. 1996, University of Kentucky Center for Computational Science, Internal Report (Lexington: Univ. Kentucky)
Ferland, G. J., & Osterbrock, D. E. 1985, ApJ, 289, 105
Francis, P. J., et al. 1996, ApJ, 457, 490
Franx, M., Illingworth, G. D., Kelson, D. D., van Doggum, P. G., & Tran, K.-V. 1997, ApJ, submitted
Gallagher, J., Hunter, D., & Tutukov, A. V. 1984, ApJ, 284, 544
Giavalisco, M., Koratkar, A., & Calzetti, D. 1996, ApJ, 466, 831
González Delgado, R. M., Heckman, T. M., Leitherer, C., Meurer, G., Krolik, J., Wilson, A. S., Kinney, A., & Koratkai, A. 1998, ApJ, submitted
González Delgado, R. M., Leitherer, C., & Heckman, T. M. 1997, ApJ, 489, 601 (Paper I)
Hartmann, L. W., Huchra, J. P., & Geller, M. J. 1984, ApJ, 287, 487
Hartmann, L. W., Huchra, J. P., Geller, M. J., O'Brien, P., & Wilson, R. 1988, ApJ, 326, 101
Heckman, T. M., & Leitherer, C. 1997, AJ, in press
Heckman, T. M., González Delgado, R. M., Leitherer, C., Meurer, G. R., Krolik, J., Wilson, A., Kinney, A. L., & Koratkar, A. 1997, ApJ, 482, 114
Hu, E. M., & McMahon, R. G. 1996, Nature, 382, 281
Hurwitz, M., Jelinsky, P., & van Dyke Dixon, W. 1997, ApJ, 481, L31
Kennicutt, R. 1983, ApJ, 272, 54
Kinney, A. L., Bohlin, R. C., Calzetti, D., Panagia, N., & Wyse, R. F. G. 1993, ApJS, 86, 5
Kinney, A. L., Calzetti, D., Bica, E., & Storchi-Bergmann, T. 1994, ApJ, 429, 172
Kruk, J. W., Durrance, S. T., Kriss, G. A., Davidsen, A. F., Blair, W. P., Espey, B. R., & Finley, D. 1995, ApJ, 454, L1
Kunth, D., Lequeux, J., Mas-Hesse, J. M., Terlevich, E., & Terlevich, R. 1997, in Rev. Mexican Astron. Astrofis. Conf. Ser., Starburst Activity in Galaxies (Vol. 6), 61
Kunth, D., Lequeux, J., Sargent, W. L. W, & Viallefond, F. 1994, A&A, 282, 709
Leitherer, C., Ferguson, H., Heckman, T., & Lowenthal, J. 1995a, ApJ, 454, L19
Leitherer, C., & Heckman, T. M. 1995, ApJS, 96, 9
Leitherer, C., Robert, C., & Heckman, T. M. 1995b, ApJS, 99, 173
Leitherer, C., Vacca, W. D., Conti, P. S., Filippenko, A. V., Robert, C., & Sargent, W. 1996, ApJ, 465, 717
Lequeux, J., Kunth, D., Mas-Hesse, J. M., & Sargent, W. L. W. 1995, A&A, 301, 18
Lowenthal, J. D., Hogan, C. J., Green, R. F., Caulet, A., Woodgate, B. E., Brown, L., & Foltz, C. B. 1991, ApJ, 377, L73
Lowenthal, J. D., Hogan, C. J., Green, R. F., Woodgate, B. E., Caulet, A., Brown, L., & Bechtold, J. 1995, ApJ, 451, 484
Lowenthal, J. D., Hogan, C. J., Leach, R. W., Schmidt, G. D., & Foltz, C. B. 1990, ApJ, 357, 3
Lowenthal, J. D., et al. 1997, ApJ, 481, 673
Maeder, A. 1990, A&AS, 84, 139
Maeder, A., & Meynet, G. 1988, A&AS, 76, 411
Malkan, M., Teplitz, H., & McLean, I. 1995, ApJ, 448, L5
Mar, D. P., & Bailey, G. 1995, Proc. ASA, 12, 239
Margon, B., Anderson, S. F., Mateo, M., Fich, M., & Massey, P. 1988, ApJ, 334, 597
Massey, P., Lang, C. C., Degioia-Eastwood, K., & Garmany, C. D. 1995, ApJ, 438, 188
McCarthy, P. 1993, ARA&A, 31, 639
Meier, D., & Terlevich, R. 1981, ApJ, 246, L109
Miralda-Escudé, J., & Ostriker, J. P. 1990, ApJ, 350, 1
Moller, P., & Warren, S. J. 1993, A&A, 270, 43
Morton, D. C. 1979, MNRAS, 189, 57
Murtagh, F., Starch, J.-L., & Bijaoui, A. 1994, A&A, 112, 179
Neufeld, D. A. 1990, ApJ, 350, 216
Pritchet, C. J., & Hartwick, F. D. A. 1990, ApJ, 355, L11
Robert, C., Leitherer, C., & Heckman, T. M. 1993, ApJ, 418, 749
Robert, C., et al. 1997, in preparation
Stark, A., Gammie, C., Wilson, R., Bally, J., Linke, R., Heiles, C., & Hurwitz, M. 1992, ApJS, 79, 77
Steidel, C., Giavalisco, M., Pettini, M., Dickinson, M., & Adelberger, K. L. 1996, ApJ, 462, L17
Steidel, C., & Hamilton, D. 1993, AJ, 105, 2017
Storchi-Bergmann, T., Kinney, A. L., & Challis, P. 1995, ApJS, 98, 103
Terlevich, E., Díaz, A. I., Terlevich, R., & García-Vargas, M. L. 1993, MNRAS, 260, 3
Thompson, D., Djorgovski, S., & Trauger, J. 1995, AJ, 110, 963
Trager, S. C., Faber, S. M., Dressler, A., & Oemler, A., Jr. 1997, ApJ, 485, 92

Vacca, W. D., Robert, C., Leitherer, C., & Conti, P. S. 1995, ApJ, 444, 647
Valls-Gabaud, D. 1993, ApJ, 419, 7
Walborn, N. R., Bohlin, J. N., & Panek, R. J. 1985, International Ultraviolet Explorer Atlas of O-Type Spectra, Nasa Reference Publication 1155 (Washington: NASA)
Walborn, N. R., Long, K. S., Lennon, D. J., & Kudritzki, R.-P. 1995, ApJ, 454, L27
Wolfe, A. M. 1995, in the Proc. ESO Conf. on QSO Absorption Lines, ed. G. Meylan (Berlin: Springer), 13
Yee, H. K., Ellingson, E., Bechtold, J., Carlberg, R. G., & Cuillandre, J.-C. 1996, AJ, 111, 1783
York, D. G. 1974, ApJ, 193, L127